國 立 交 通 大 學

應用化學系碩士班

碩 士 論 文

飛秒雷射誘發光學熔損製備金與銀奈米粒子

Gold and silver nanoparticles fabrication by femtosecond

laser-induced optical breakdown

研 究 生：王 順發 (Shun-Fa Wang)

指導教授：三浦 篤志 博士 (Dr. Atsushi Miura)

中 華 民 國 一 百 零 一 年 七 月

飛秒雷射誘發光學熔損製備金與銀奈米粒子

Gold and silver nanoparticles fabrication by femtosecond

laser-induced optical breakdown

研 究 生：王順發　　　　　Student：Shun-Fa Wang

指導教授：三浦 篤志 博士　　Advisor：Dr. Atsushi Miura

國 立 交 通 大 學
應用化學系碩士班
碩 士 論 文

A Thesis
Submitted to M.S. Program
Department of Applied Chemistry
National Chiao Tung University
in partial Fulfillment of the Requirements
for the Degree of
Master
in

Applied Chemistry

July 2012

Hsinchu, Taiwan, Republic of China

中 華 民 國 一 百 零 一 年 七 月

Gold and silver nanoparticles fabrication by femtosecond laser-induced optical breakdown

Student: Shun-Fa Wang   **Advisor: Dr. Atsushi Miura**

M.S. Program
Department of Applied Chemistry
National Chiao Tung University

Abstract

When femtosecond laser pulses are focused into water, an impulsive force is generated that propagates from the laser focal point in a micron-sized space. This femtosecond laser-induced optical breakdown has been widely used as a promising technique for detaching and manipulating individual adherent cells, and insertion of nanoparticles and bio-molecules into cells. In early studies on the femtosecond laser application, most researchers have focused only on the induced physical behaviors, but rarely on chemical aspect of the behaviors such as generation of transient chemical species by the irradiation. The investigation of the chemical reactions on femtosecond laser-induced multiphoton absorption in solution is indispensable to confirm that these physical behaviors are realized without any chemical changes.

In this work, gold and silver nanoparticle fabrication is chosen as a probe in order to confirm the generation of transient species such as ions and radicals by intense femtosecond laser irradiation, since the resultant metal nanoparticles shows these

characteristic extinction spectra due to their surface plasmon. These nanoparticles are prepared by the multiphoton reduction of $HAuCl_4$ and $AgNO_3$ in the presence/absence of polyvinylpyrrolidone (PVP) and/or 1-propanol, and the formation of colloid formation is confirmed by the change in the extinction spectra.

The laser energy dependence of gold nanoparticle formation strongly supports the reduction of $HAuCl_4$ through 2-photon absorption of $AuCl_4^-$. On the other hand, for silver nanoparticle formation, the increase in the Δextinction is observed only in the presence of PVP, which indicates that the colloid formation is achieved through the 2-photon absorption of PVP. While, even in the absence of PVP, a little extinction change is observable. This result suggests that silver ions are reduced by hydroxyl and/or hydrogen radicals due to 4-photon absorption of water, that is due to femtosecond laser-induced optical breakdown.

Thus, we successfully demonstrate multiphoton absorption of $AuCl_4^-$, PVP and H_2O by femtosecond laser irradiation as a primary mechanism of gold and silver nanoparticle fabrication. Furthermore, we have succeeded in nanoparticle fabrication by laser ablation of nanoparticles formed by the reduction, and also succeeded in controlling the mean size and the size distribution by optimizing various kinds of experimental conditions. These successes will give us a novel guideline for the studies on femtosecond laser-induced phenomena.

飛秒雷射誘發光學熔損製備金與銀奈米粒子

研究生：王順發　　　　　　　　　　　指導教授：三浦篤志 博士

國立交通大學 應用化學系碩士班

摘要

　　當飛秒雷射脈衝聚焦在水中，會在微米大小的雷射焦點產生一股斥力並向外擴散，這種飛秒雷射誘發光學熔損廣泛地應用在一些很具發展性的科技上，如分離和操作獨立附著的細胞以及嵌入奈米粒子與生物分子進細胞內，近年在飛秒雷射應用的研究上，研究人員只專注在雷射產生的物理作用上，鮮少探討化學方面的作用，例如雷射照射下短暫物質的生成，因此，飛秒雷射在溶液中誘發多光子吸收產生化學反應的研究對於證明雷射誘發的物理作用與化學作用是相當重要的。

　　在我們的研究中，金奈米及銀奈米粒子的製備可以當成是探測的工具，藉由生成的金屬奈米粒子因表面電漿共振所展現的消光光譜，可證實飛秒雷射照射下所生成的離子和自由基等短暫物質，這些奈米粒子是藉由四氯金酸與硝酸銀在溶液中的多光子還原來製備，奈米粒子膠體溶液的形成可由消光光譜上的變化而得知。

　　雷射能量相關的作圖可以推測四氯金酸的還原是透過四氯金酸離子的雙光子吸收來進行，對銀奈米粒子的製備而言，消光光譜的強度只在聚乙烯吡咯烷酮存在的溶液中大量增加，從這可以得知聚乙烯吡咯烷酮的雙光子吸收造成還原反應的發生，然而在沒有聚乙烯吡咯烷酮的硝酸銀溶液中仍然可觀測到少量的光譜

變化，這結果可推論水的四光子吸收，也就是飛秒雷射誘發光學熔損所生成的氫原子自由基與氫氧自由基可以還原銀離子。

因此，透過四氯金酸、聚乙烯吡咯烷酮及水在雷射照射下的多光子吸收，我們推導出金奈米及銀奈米粒子還原的機制，此外，雷射熔損也可控制奈米粒子的製備，根據不同的實驗參數，我們也成功地控制奈米粒子的大小與粒徑分佈，這研究將會成功且創新地引導未來飛秒雷射誘發現象的發展。

Acknowledgement

I am very glad and fortunate to join our laboratory, Laser Bio/Nano Science Laboratory, where I have opportunity to operate the advanced optical equipment, investigate the novel research and cooperate with many intellectual scholars, as my master student career in these two years. I sincerely appreciate Prof. Hiroshi Masuhara for giving me new experimental ideas and teaching me how to explore scientific world patiently. Even in daily life, a lot of encouragement and support for us are covered in a joke or routine communication, leading us to learn the positive attitude.

I must express many thanks to Dr. Takayuki Uwada who advises my experiment and offers opinions to me. Such nice experimental environment organized by Prof. Atsushi Miura is essential to be mentioned and praised. I deeply appreciate Prof. Teruki Sugiyama for revising my master thesis and discussing my experiments. With the help of Prof. Sugiyama for my master thesis, I can graduate successfully on time.

Many thanks to senior members inclusive of Dr. Anwar Usman, Dr. Ken-ichi Yuyama, Mrs. Wen-Yu Lee, Mr. Ping-Yu Hee, Ms. Jing-Ru Tu, Mr. Chong-Wei Huang and Mr. Tsung-Han Liu, my classmate Mr. Wei-Yi Chiang, Mr. Tsu-Wei Hsu, Ms. Ling-Ting Huang, Mr. Yan-Hua Huang and Mr. Ching-Hsu Tseng, and junior member Mr. Chi-Shiun Wu. We have a great corporation in a nice atmosphere.

Table of Contents

List of Figures

1. Introduction

Various laser techniques have been developed widely since the 1960s due to the unique properties of laser light. The high spatial coherence of laser light permits directional irradiation and excellent focusing. The monochromaticity of laser light allows us for highly selective narrow-band excitation [1]. For pulsed lasers, the extremely high energy density can be achieved within each laser pulse ranging from the nanosecond to femtosecond scale. Until now, applications of their lasers are expanded broadly in physics, chemistry, biology and industry. Laser-induced crystallization is one of the important researches among applied laser developments. Laser-induced crystallization can be divided to "Laser trapping crystallization" and "laser tsunami crystallization" according to different laser irradiation modes.

In "laser trapping crystallization", molecules and/or clusters in solution are trapped at the focal point by photon pressure of a focused intense near-infrared continuous wave laser irradiation, the local concentration increases, and crystal nucleation is eventually triggered. Generally, laser trapping technique is used for manipulating micrometer-sized objects without any mechanical contact but with interactions between photons and the target objects. Sugiyama *et al.* for the first time demonstrated laser trapping crystallization of glycine in 2007 [2].

On the other hand, in "laser breakdown-induced crystallization", the focused intense near-infrared femtosecond laser pulses irradiates into solution and induces optical breakdown by multiphoton absorption of water involving nonlinear phenomena like shockwaves, cavitation bubbles and jet flow. The local physical perturbations of laser tsunami trigger nucleation, and crystallization.

Among various pulsed lasers, femtosecond laser attracts much attention because of its high potential applications of short and high photon density pulse, for example, in the research fields of imaging, processing[1, 3], optical communication, and biomedicine[3-4] and so on. When the femtosecond laser pulses are focused through an objective lens with high N.A. into water, an impulsive force is generated, which propagates from the laser focal point to a micro-sized space. This force can detach individual adherent cells from a substrate without considerable cell damage, and using this laser-induced optical breakdown, the manipulation of a large living cell and insertion of nanoparticles into cells have been demonstrated so far. However, these studies have been carried out under the assumption that no chemical reaction takes place by femtosecond lase irradiation, that is, only physical phenomena is considered.

On the other hand, one of the most profitable behaviors of short high-intensity laser pulses is laser ablation. When the pulse laser with intensity above a threshold focuses on a solid substrate, fragmentation of the substrate is induced. The laser

ablation has been discussed on the basis of thermal, mechanical, photophysical, photochemical, and defect model [1]. The process starts through one-photon or multiphoton absorption of target materials. If the excitation energy is converted to heating instantaneously, temperature elevation causes rapid volume expansion and following mechanical crash, resulting in thermal material ablation (vaporization) with or without melting. Another phenomenon related to temperature elevation is formation of thermally induced defects. This overall process is regard as "thermal ablation". If photon energy is high enough, laser-light excitation can break chemical bondings with the assumption that bond change is faster than non-radiative relaxation. The process is so-called "photochemical ablation". When both thermal and photochemical mechanisms contribute to the ablation, the generation of defects, stresses, and volume changes influence the overall process, which is considered as "photophysical ablation".

In this research, we consider the generation of chemical transient species through the gold and silver nanoparticle fabrication by femtosecond laser irradiation. The detail mechanisms processes during femtosecond laser irradiation shall be mentioned and examined in our experiments.

1.1 Research purpose

In this work, we first aim the confirmation of the transient chemical species generated by femtosecond laser irradiation of 800 nm into solution. We chose $HAuCl_4$ and $AgNO_3$ aqueous solution as starting samples, and confirm the generation of their chemical species through the corresponding nanoparticle preparation of Au and Ag, respectively. Since $HAuCl_4$ and $AgNO_3$ have surely no photon absorbance at 800 nm, their nanoparticle formation should require the multiphoton reduction of $HAuCl_4$ and $AgNO_3$. There, we examine the laser energy dependence of gold and silver nanoparticle formation and reveal the reduction process of $HAuCl_4$ and $AgNO_3$ through the multi-photon absorption. In addition, we confirm laser ablation behavior of the formed nanoparticles by the further irradiation and try to control their mean size and their distribution by optimizing various experimental conditions such as laser energy, solution concentration, and additives.

1.2 Why metallic nanoparticle preparation is studied?

Noble metallic nanoparticles have collected much interest for past two decades because they exhibit strong light scattering and absorption in visible region due to surface plasmon resonance. The surface plasmon resonance is the coherent excitation

of all the free electrons within the conduction band, leading to an in-phase oscillation.

For the particles with size of several tens of nanometers which is smaller compared to

incident light wavelength, excitation of surface plasmon resonance can be induced

with visible light. As a result, the particles possess strong light scattering and

absorption in visible region. On the other hand, the surface is very important for the

observation of the surface plasmon resonance, as it alters the boundary conditions for

the polarizibility of the metal and therefore shifts the resonance to optical frequencies[5].

It means that the optical properties depend on the size and shape of metal and can be

applied to intense electromagnetic field enhancement [4a, 6].

Besides, the reduction of metal nanoparticle is much simple and easy to explore

transient species, because only reduction product, i.e., metal is enough to be

considered, while many complicated reactions take place in organic molecules. Metal

nanoparticles are relatively stable and convenient to measure and analyze by UV-Vis

absorption spectroscopy. Therefore, the fabricated metal nanoparticles are examined

to elucidate transient species and reactions due to femtosecond laser induced

multiphoton absorption.

Fig.1.1 The gold nanoparticles with different sizes show various colors[6].
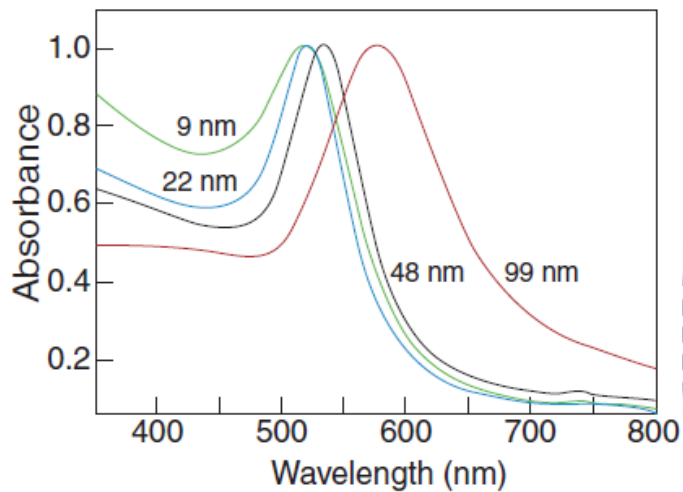
Fig.1.2 The absorption spectra of surface plasmon of gold nanoparticle demonstrate size dependence[4a].

1.3 General preparation method of metallic nanoparticles

1.3.1 Top-down method

1.3.1.1 Electron beam lithography

The electron beam lithography tool achieves an accurate control for ultrahigh resolution mask-making, direct writing and metallic nanostructure fabrication [7]. For

6

metallic nanoparticles and nanowire fabrication of liftoff process, the designed pattern

is written with electron beam into a 100 nm thick PMMA (poly-methyl-methacrylate)

resist layer which is spin-coated on ITO (indium-tin oxide) doped glass substrate.

After the exposed resist layer is removed, the metal vapor is coated on the surface of

both unexposed the resist layer and exposed resist layer. Finally, the unexpected area

is taken off by liftoff process, and a designed nanostructure is obtained [8]. Generally,

the electron beam lithography can provide the demand of well shape and specific

structure. The exact control is achieved by this method and used in photolithography.

Nonetheless, the limitations of electron beam lithography such as long working time

and low production yield results in restricted application and investigation.
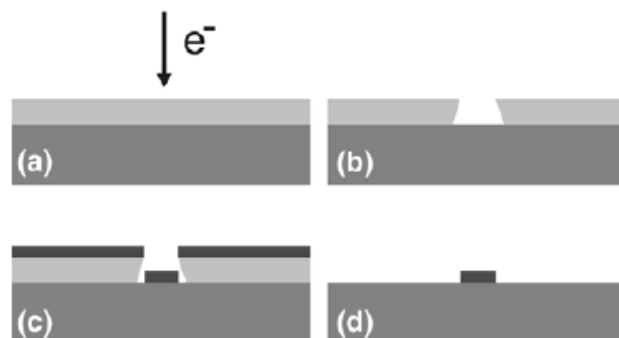
Fig.1.3 The principle of e-beam lithography process for the fabrication of nanostructure. (a) & (b) e-beam irradiation on PMMA resist layer with thickness of 100 nm, which spin-coated on ITO glass substrate. (c) Vacuum decomposition of metal, and (d) removal at unexposed area by the liftoff process[8].

1.3.1.2 Laser ablation

Pulsed laser ablation of a target of a solid substrate immersed in aqueous solution

can induce the fragmentation resulting in reduction in the size over time, which

process is regarded as "Top-down" method for the nanoparticle preparation[9]. The

obtained nanoparticles can be fabricated mechanically, physically or chemically. The

most beneficial advantage of this method is the fact that high purity nanoparticle

without other residual ions is fabricated[10]. On the contrary, the disadvantage of this

method is the low production yield, which makes it difficult to accumulate sufficient

concentration of nanoparticles, and wide size distribution of nanoparticles is found.

1.3.2 Bottom-up reduction method

1.3.2.1 Chemical preparation method of metallic nanoparticle

The method of conventional metallic nanoparticles synthesis is chemical

reduction by adding reductants into the metallic ion solution. One of the most

well-known chemical reduction methods for gold nanoparticles is Turkevich method

established by Turkevich *et al*. and refined by Frens [11]. The almost spherical

nanoparticles with wide tunable range of size can be obtained in the reducing process

in the presence of sodium citrate. The stabilization of nanoparticles is assisted by

surfactants which also determine geometrical shapes of the nanoparticle such as rod,

cube, and triangle and so on. For instant, nanorod particles can be gotten in the

surfactant, cetyltrimethylammonium bromide (CTBA) mixed in ascorbic acid and metallic ion solution. In addition, other reductants, for example amino acids, are successfully reducing gold nanoparticles without any surfactants and the shape is determined by the reductants. In this method, it is found that the relation between gold/citrate ratio and final size. The obtained gold nanoparticles can be kept for a long time and maintained stable state.

The other method discovered by Brust *et al*. can produce gold nanoparticles in a two-phase system, liquid-liquid (water-toluene) [12]. The chlorauric acid is mixed with tetraoctylammonium bromide (TOAB) solution in toluene and sodium borohydride solution. TOAB is not only the phase transfer agent but also the stabilizing agent. Sodium borohydride in this system is a reducing agent and dodecanethiol is added to the solution in order to prevent gold nanoparticles from aggregating. In this method, the gold nanoparticles have a diameter distribution in the range of 1-3 nm and the size distribution profile peak is 2-2.5 nm approximately.

For Turkevich method and Brust method, the gold particle size range is 12-100 nm and 2-10 nm respectively. It is hard to obtain high quality spherical gold nanoparticles whose size is up to 50 nm. In 2009, a seed-based method was published by Perrault *et al*. and it is important that this method can produce gold nanoparticles with united shape and identical size. The gold nanoparticles in identical size can be

tunable in the range from 50 nm to 200 nm [13].

1.3.2.2 Sonication method of metallic nanoparticle reduction

It is well known that sonication has been utilized and applied for several decades. The synthesis method of sonication-induced nanoparticles reduction has been developed in the field of sonochemistry and applied to Au, Ag, Pt, Tl, Fe, MnO_2 and CdS and so on[14]. The high intensity ultrasonic irradiation through aqueous solution generates a series of bubble formation called "cavitation". The cavitation bubble formation includes 3 processes, bubble expansion, bubble collapse and light emission, leading to extreme high temperature and pressure within the bubble [15]. Initially, the cavitation bubble absorbs energy offered by ultrasound and then expands toward the maximum size in which the temporally low pressure is attained. The cavitation bubble collapse creates sharply rising in temperature and pressure due to near-adiabatic compression. Finally, the energy of the cavitation bubble converts to mechanical energy, heat, chemical reaction and light emission. Barber *et al*. published that the light emission from single bubble can include more than 10^7 photons per flash [16]. Flannigan and Suslick observed the emission spectra from which the temperature upon 15,000 Kelvin was estimated through the collapsing bubble [17]. During the process of cavitation bubble collapse, high density plasma (ionized gas) contained

inside the bubble undergoes formation of radicals and ions, which may diffuse to the solution along the border of bubble. This radicals and ions possess high reducing ability [18].

When water is sonicated by ultrasound, dissociation of water to hydrogen radicals and hydroxyl radicals take place due to extremely high temperature in collapsing cavitation bubble. However, the lifetime of hydrogen radicals and hydroxyl radicals are roughly as short as 10^{-7} second order. Hydrogen radicals and hydroxyl radicals are possible to encounter with each other, resulting in recombination reactions whose products are hydrogen, water and hydrogen peroxide. Hence, alcohol is added to the solution as intermediate whose lifetime is much longer. Alcohol attacked by hydrogen radicals and hydroxyl radicals at the cavitation bubble can form alcohol radicals and act as a radical scavenger that can prevent recombination reaction owing to diffusion in solution. No matter what kind of alcohols are involved in the reaction, such as methanol, ethanol, 1-propanol or 1-pentanol, alcohol radicals show high performance in reduction of metallic ions. It is reported that longer carbon chain alcohol owns better reducing ability of gold nanoparticles by Caruso *et al.* [19]. The average particle size shows decreasing trend with increased in alcohol concentration and alkyl chain length

1.3.2.3 Radiation-induced formation of metallic nanoparticle

The gamma ray irradiation induced synthesis of metallic nanoparticles, which is based on formation of reactive transient species triggered by ^{60}Co source. Reactive transient species like electrons, hydrogen radicals and hydroxyl radicals can be produced through water radiolysis. For the reduction of gold ions, alcohol ought to be present necessarily in aqueous solution and scavenge reactive transient species efficiently, which generates alcohol radicals with high reduction potential [20]. Gold nanoparticles synthesis is completed approximately after 10 hours irradiation in the presence of methanol at a dose rate of 1.8×10^4 rad/h [21].

Another method of radiation-induced formation of metal nanoparticles is UV photoactivation. The UV photoactivation technique is able not only to reduce noble metal ions solution but also to stimulate the growth of seed-base nanoparticles along certain direction or on their surface like "core-shell" type nanoparticles [22]. The UV photoactivation usually occurs with the functional groups such as sodium alginate which acts as a stabilizer and a reducing agent [23]. On the other hand, the nanoparticles enlargement is achieved in the seed nanoparticles solution by UV light irradiation. When the UV light irradiation is collimated through the seed nanoparticle solution, their distribution grew up along the direction of UV light and hence this method can be expanded to nanorod synthesis. In the further exploration, the seed mediated

formation of bimetallic nanoparticles for the preparation of "core-shell" structure

nanoparticles is come out by UV light irradiation [24].

There are certain advantages utilizing these radiolysis techniques as compared to

conventional chemical and photochemical methods: (1) Excess reducing agent and

undesired oxidation products are not necessary. (2) Reaction rate has been already

established because the number of reducing equivalents is well defined. (3)

Absorption of irradiation in the presence of light-absorbing solutes and products is

regardless. (4) Generation of the reducing agent is spatially uniformed [21]

2. Principle

2.1 Plasmon resonance

The scientific investigations on the optical properties of metal nanoparticles originated from Faraday in 18th century. When a small spherical metal nanoparticle is irradiated by an electromagnetic wave, the oscillating electric field shifts electrons in conduction band collectively with respect to fixed positive charge, causing conduction electrons to oscillate coherently. Fig. 2.1 is schematically showing the displacement of the conduction electron charge cloud relative to the nuclei. A restoring force is formed due to Coulomb attraction between the negative and positive charges on the opposite side. The electron cloud is displaced relative to the nuclei resulting in the oscillation of electrons and nuclei. This collective oscillation of conduction electrons is called "plasmon resonance" [6a, 25].

The oscillation frequency is determined by 4 factors; the density of electrons, the effective electron mass, and the shape and size of charge distribution. For silver, the plasmon frequency is also influenced by other electrons, making it difficult to calculate the plasmon frequency. In order to relate the plasmon frequency to the metal dielectric constant which is a function of wavelength, we consider the interaction of light on spherical particle which is much smaller than wavelength of light. Under

these circumstances, the electric field of light is constant and the interaction is governed by electrostatics. The wavelength-dependent dielectric constants of the metal particles, ϵ_i and of the surrounding medium, ϵ_0 are depicted in electrostatic theory. To determine the electromagnetic field surrounding the particles, we have to solve the Laplace equation, $\nabla^2 \varphi = 0$, where φ is the electric potential and the electric field of incident electromagnetic wave E is related to φ by $E = -\nabla\varphi$. The boundary conditions are that φ is continuous at the sphere surface and that the normal component of the electric displacement D is also continuous.

For a sphere, the Laplace equation solution exhibits that the polarizability is

$$\alpha = g_d a^3$$

with

$$g_d = \frac{(\epsilon_i - \epsilon_0)}{(\epsilon_0 + 2\epsilon_0)}$$

and a is the radius of sphere. The more complete Maxwell equation solution can contribute to extinction and Rayleigh scattering by the sphere. This leads to extinction and scattering efficiencies given by

$$Q_{ext} = 4x Im(g_d)$$

$$Q_{sca} = \frac{8}{3} x^4 |g_d|^2$$

where

$$x = 2\pi a (\epsilon_0)^{1/2} / \lambda$$

15

The efficiency is the ratio of the cross-section to the geometrical cross-section πa^2. g_d is an important factor for determining the wavelength dependence of these cross-sections because the metal dielectric constant ϵ_i is strongly dependent on wavelength.
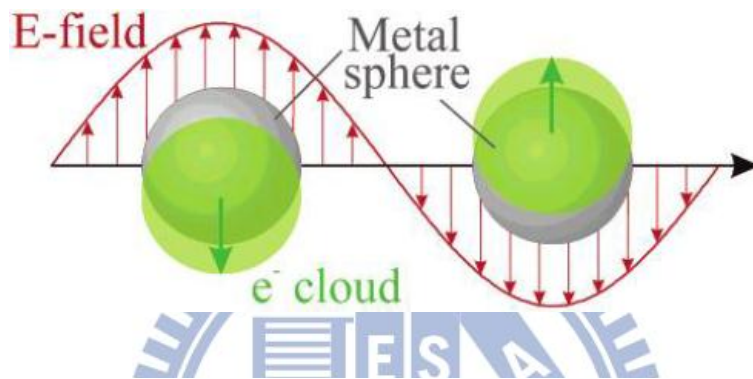
Fig.2.1 Scheme of plasmon oscillation for a sphere[4a].

2.2 Femtosecond laser

Amplified Ti:sapphire femtosecond laser is the combination of a mode-locked Ti:sapphire laser, Empower laser and Ti:sapphire regenerative amplifier system. A mode-locked Ti:sapphire laser (wavelength: 700-900 nm, repetition rate: 80 MHz, pulse duration: 160 fs, Tsunami, Spectra Physics) as a seed laser provides the input pulse to the amplified Ti:sapphire femtosecond laser. A diode-pumped continuous wave visible laser (wavelength: 532 nm, Millenia Pro, Spectra Physics) supplies 7 W to pump Ti:sapphire rod in the cavity of mode-locked Ti:sapphire laser which is controlled by an electronics module (Model 3955, Spectra Physics). The full width at

half maximum (FWHM) of the spectrum and central wavelength of the laser light are determined to 12.5 nm and 800 nm, respectively. Acousto-optics modulator (AOM) ensures proper mode-locked pulsing at the period of laser operation. The output wavelength can be tuned by a slit wavelength selector and overall cavity dispersion balance as well as shortest output pulse can be adjusted by a prism dispersion compensation control.

The high peak power compressed pulse coming from the amplified Ti:sapphire femtosecond laser is ascribed to 3 individual step; stretcher, amplifier, and compressor. Firstly, the low-power, short-duration pulse from Tsunami seed laser is stretched so that it lasts longer time based on the principle of group velocity dispersion (GVD) or informally "chirp". The short pulse is lengthened by the device which can delay longer wavelengths, leading to the generation of wide wavelength spreading but reduction of peak power pulse. Secondly, a synchronous energy pulse of Empower laser amplifies the energy of the stretched pulse. Thirdly, the compressor uses a horizontal retroreflector to force the longer wavelengths to take longer path, causing pulse duration tends to original length. The amplified laser pulse possesses high peak power and short duration time simultaneously. These 3 step are completely performed in Ti:sapphire regenerative amplifier system (Spitfire Pro, Spectra Physics).

However, when the intense laser beam passes through a Ti:sapphire crystal, a

nonlinear optical effect, self-focusing, may cause permanent damage on the crystal, because the refractive index of the crystal is modified as a result of beam focusing and intensification further. Self-focusing limits the peak power of a pulse in the Ti:sapphire crystal lower than 10 GW/ cm^2. So, chirped pulse amplification (CPA) is developed to allow the amplified pulse to pass through Ti:sapphire crystal safely below the damage threshold, meanwhile, to maintain this peak power. The 3 steps mentioned above are included in chirped pulse amplification.

Fig.2.2 A picture of mode-locked Ti:sapphire laser, Tsunami**.**
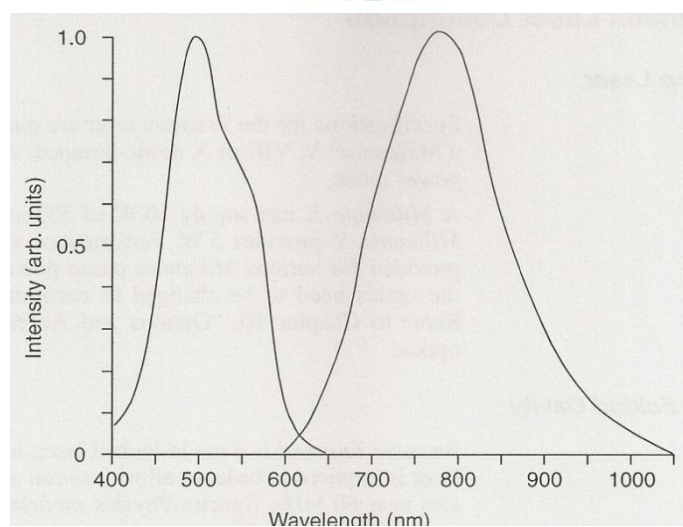
Fig.2.3 Absorption and emission spectra of Ti:sapphire**.**
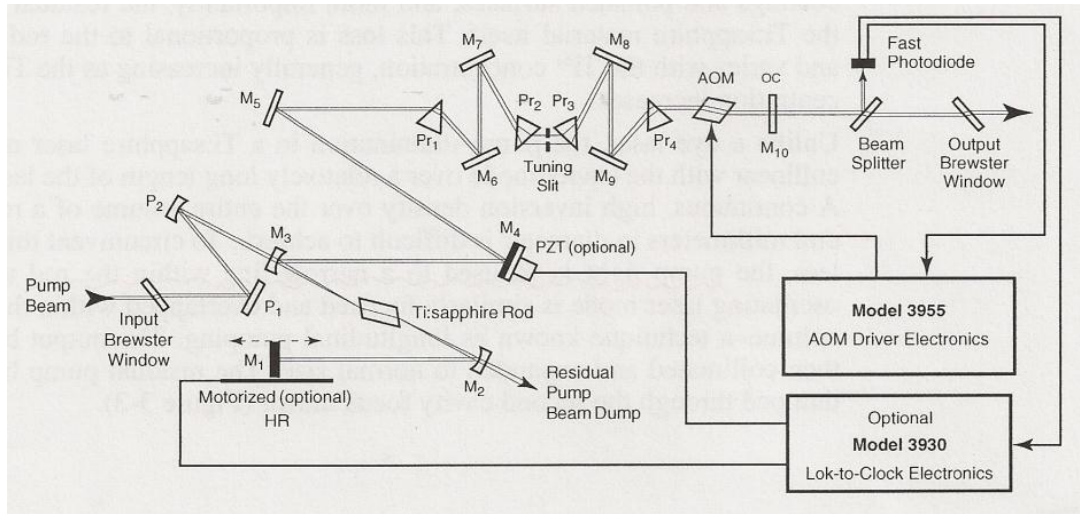
Fig.2.4 The mode-locking principle in Tsunami.

Fig.2.5 A picture of Ti:sapphire regenerative amplifier system, Spitfire
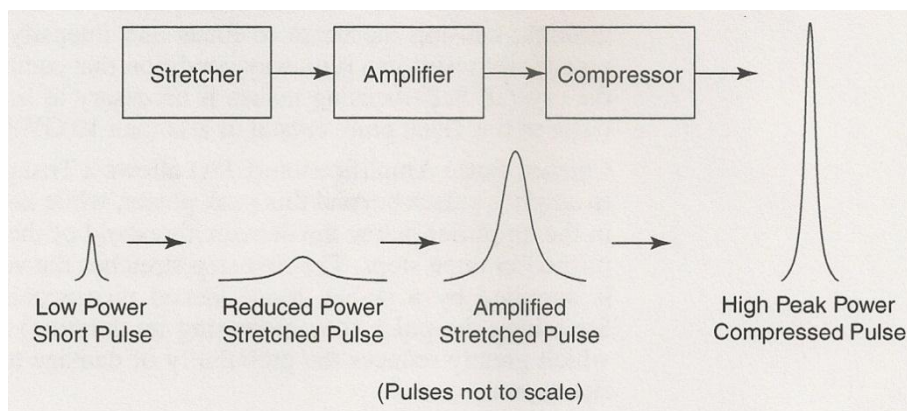
Fig.2.6 The schematic illustration of CPA principle.

2.3 Optical breakdown

Optical breakdown is associated to the laser ablation which happens above a certain threshold in air or liquid. The critical optical breakdown threshold for air calculated by Paschen curve is 30 kV/cm at 1 atm. In water, a much higher voltage of the well-accepted value of 30,000 kV/cm is necessary because of the larger density of water [26]. At the first, because the energy of single photon is insufficient to excite a molecule from ground state to excited electronic state, the energy of absorption by the molecule must be more than that of one photon. The accumulation of the energy of photons equals to the total energy of absorption between two states. Focusing intense pulse laser into water causes multiphoton absorption of water, although water does not absorb the light of the laser wavelength [27]. When increasing pulse laser energy intensity, a great deal of fraction of atoms and molecules undergoes ionization. As a consequence, a very high concentration of active intermediate species (e.g., ions, electrons, radicals, atoms, photons, and excited states) is produced around the focal position. Optical breakdown of water via multiphoton absorption is a nonlinear phenomenon in which cavitation bubble generation, shockwave propagation, and jet flow are included[28].
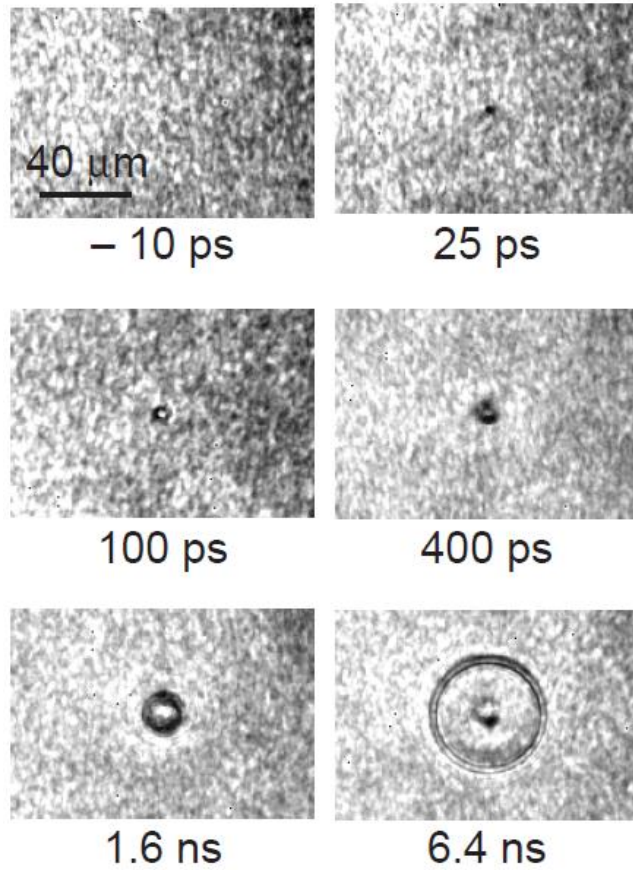
Fig.2.7 Images of femtosecond laser-induced optical breakdown in water with various time delays[28a].
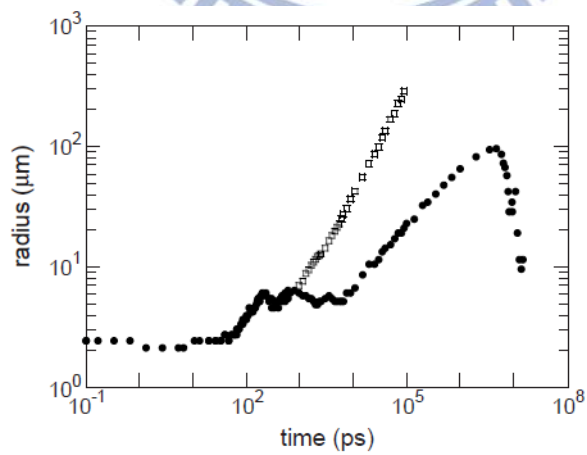
Fig.2.8 Evolution of the radius of the laser-produced plasma, pressure wave, and cavitation bubble as a function of time (● plasma/bubble radius, ❑ pressure wave)[28a].
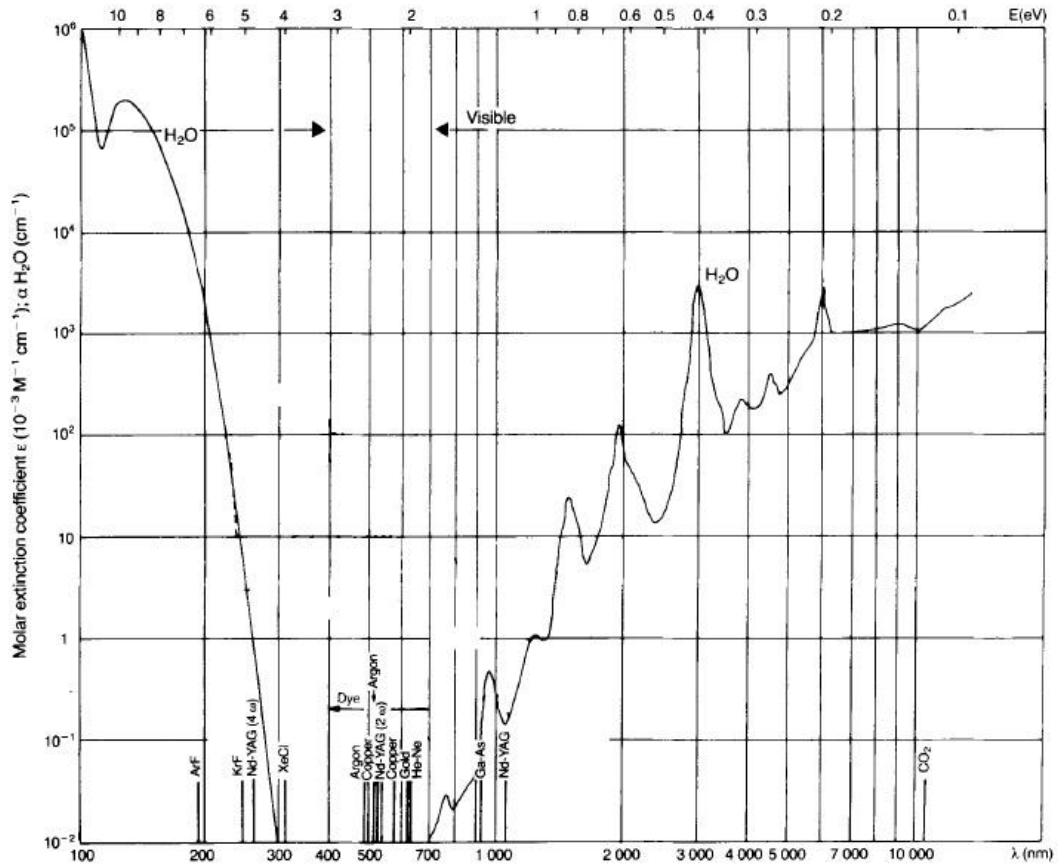
Fig.2.9 Absorption coefficient spectrum of water, together with the wavelength positions of the most widely used lasers[27].
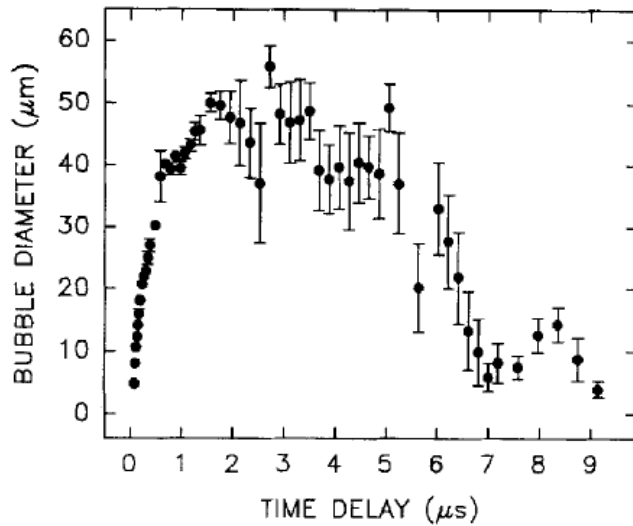
Fig.2.10 The diameter of cavitation bubble in water plotted as a function of time[28b].

22

3. Experiments

3.1 Sample preparation

3.1.1 HAuCl$_4$ solution

Hydrogen tetrachloroaurate (HAuCl$_4$) solution was prepared by dissolving gold

chloride trihydrate (Au 49.5%, Sigma-Aldrich) powder in deionized water. 0.5 mM

aqueous HAuCl$_4$ of 2 ml were poured in a quartz cell (10 mm path length, Starna) and

extra 0.1 ml 1-propanol was added. HAuCl$_4$ solution in quartz cell is shown in Fig.3.1

and the solution is pale yellow.
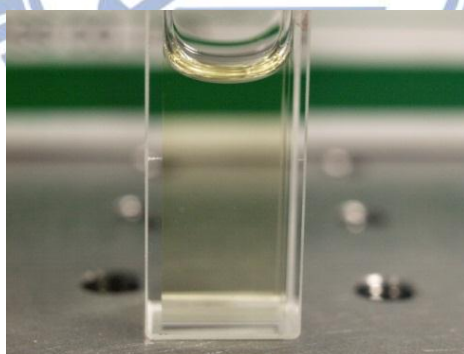
Fig.3.1 HAuCl$_4$ solution in a quartz cell

3.1.2 AgNO$_3$ solution

Silver nitrate (AgNO$_3$) (99.0%, Sigma-Aldrich) powder was dissolved in 2 ml polyvinylpyrrolidone (PVP) (molecular weight: 10,000; Sigma-Aldrich) solution which contained 20 mg PVP. The AgNO$_3$ solution concentration was adjusted to 1 mM and put into a quartz cell. AgNO$_3$ solution in quartz cell and polyvinylpyrrolidone (PVP) chemical structure are shown in Fig.3.2. The solution is transparent.
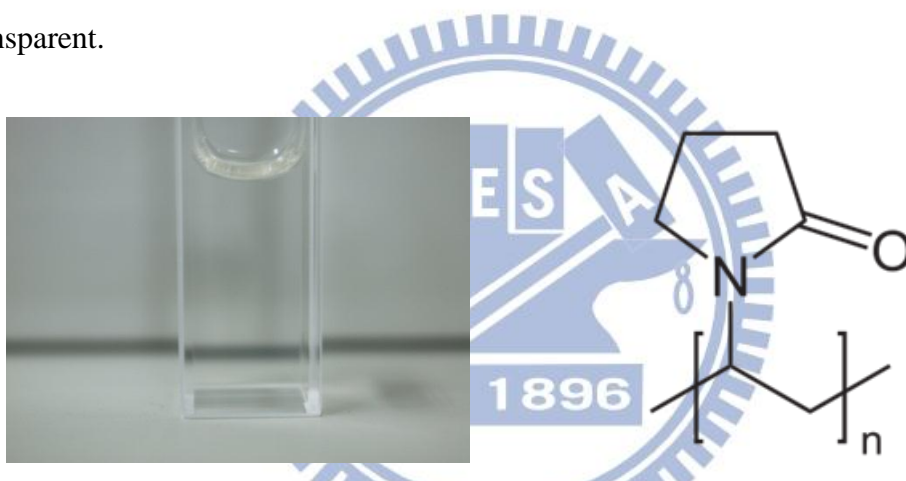
Fig.3.2 AgNO$_3$ solution in a quartz cell (left) and polyvinylpyrrolidone (PVP) chemical structure (right).

3.2 Instruments

3.2.1 Femtosecond laser

The experimental setup is shown in Fig. 3.3-Fig. 3.6. Linearly polarized femtosecond laser pulses from amplified femtosecond laser (wavelength: 800 nm, pulse duration: 160 fs, Spitfire Pro, Spectra Physics) are transmitted to an inverted

microscope (IX-71, Olympus) via an objective lens (10X, N.A. 0.25, PlanN, Olympus). Pulse energy can be adjusted by a half-wave plate, a polarizing beam splitter, and a variable neutral density filter. Pulse energy is measured beyond an objective lens by a power meter (842-PE, Spectra Physics). The repetition rate and polarization of femtosecond laser pulse train is controlled by a Pockels Cell which acts as a quarter waveplate, respectively. The conditions of all the experiments are maintained at room temperature (24℃) and one atmosphere.
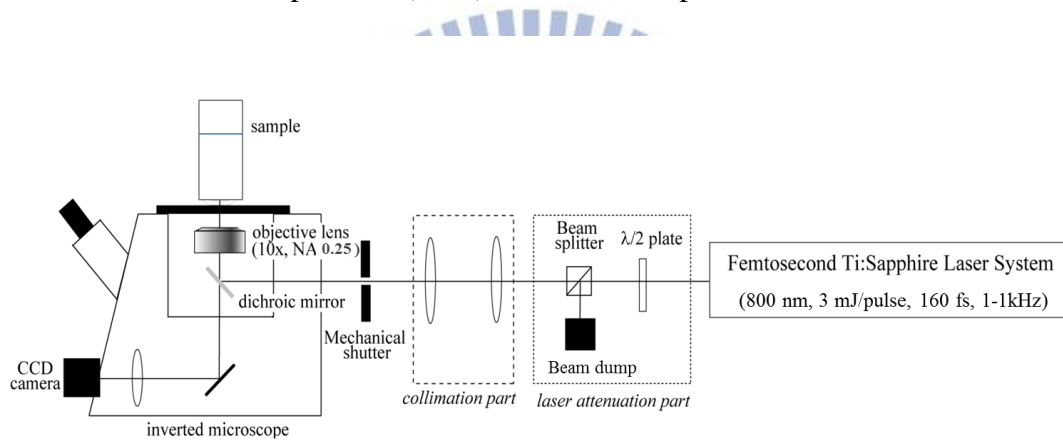
Fig.3.3 Laser light source and microscopic system.

Fig.3.4 A picture of inverted microscope and other attachments.
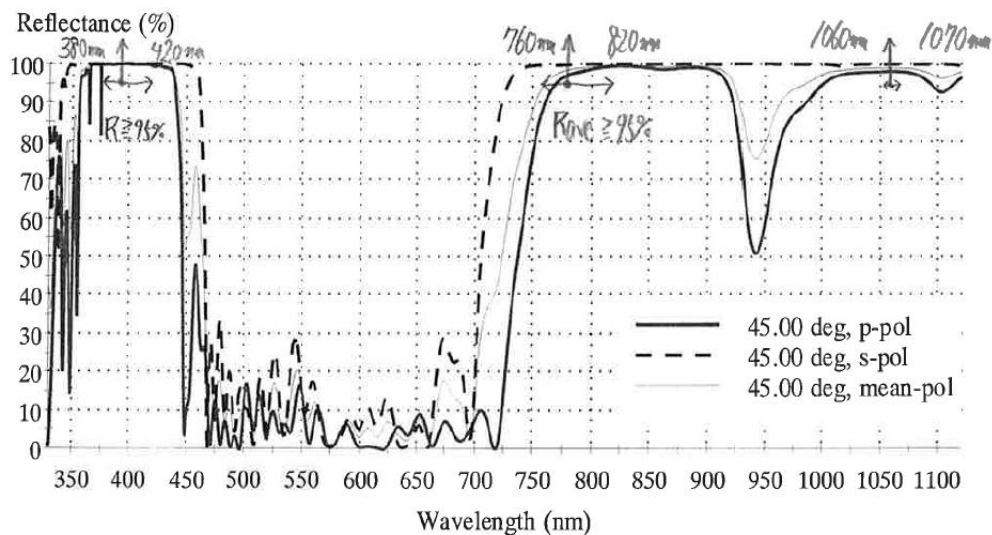
Fig.3.5 Reflectance spectrum of the dichroic mirror used in the inverted microscope.
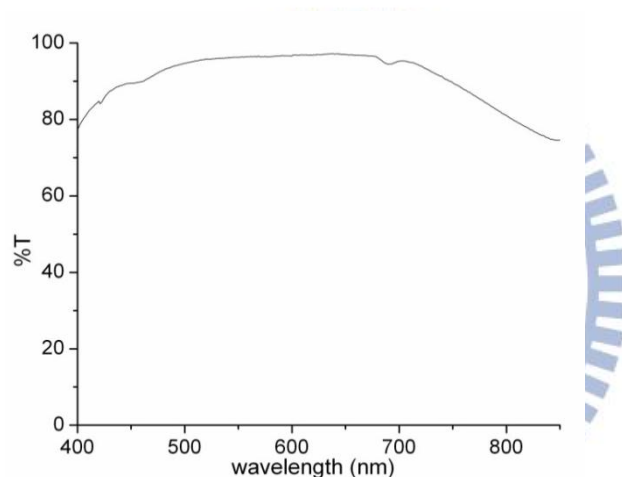
Fig.3.6 Transmittance spectrum of the objective lens used in the inverted microscope.

3.2.2 UV-Vis absorption spectroscope

The UV-Vis absorption spectra are measured by a spectrophotometer (V-670, wavelength: 190-2700 nm, JASCO). The light source comes from a deuterium lamp and a halogen lamp. The scanning range starts from 800 nm to 200 nm and the cell path length is set as 10 mm. Deionized water in quartz cell is measured as a baseline before sample scanning.

3.2.3 Scanning Electron Microscope

The equipment of scanning electron microscope (SEM) (JSM-7401F, JEOL) incorporates a cold cathode field emission gun, ultra high vacuum, and sophisticated digital technologies for high resolution imaging of nanostructure. The SEM measurement taken at 10 kV enables to observe the real surface structure while the patented gentle beam method helps to eliminate charging of non-conductive sample.

The silicon wafer was segmented to approximately 1 cm^2 piece. The plasmon processing could remove organic contaminations and particles on the surface for adherence of nanoparticles. After that, the silicon wafer section was sunk in 1 M hydrochloric acid for 10 min for removing metal ions. The treated silicon wafer could be used after washing by deionized water and drying by nitrogen gas. The sample solution was dropped down on the treated silicon wafer and was dried repeatedly and the frequency depended on the concentration of sample solution. Finally, we attached the silicon wafer on the copper holder on which a copper conductive tape (TED PELLA) and a carbon conductive tape (TED PELLA) were pasted. The graphite paint (PELCO) spread in the edge of silicon wafer smoothly in order to increase electric conductivity and fix silicon wafer well.

3.2.4 Transmission Electron Microscope

Transmission electron microscope (TEM) (JSM-2100F, JEOL) is a field emission microscope. The highest image quality can be achieved in the 200 kV class with a probe size under 0.5 nm. The preparation for TEM measurement is that a copper grid (200 mesh, TED PELLA) was sunk in the sample solution for few seconds. Then the copper grid was dried and kept in dried ambient space.
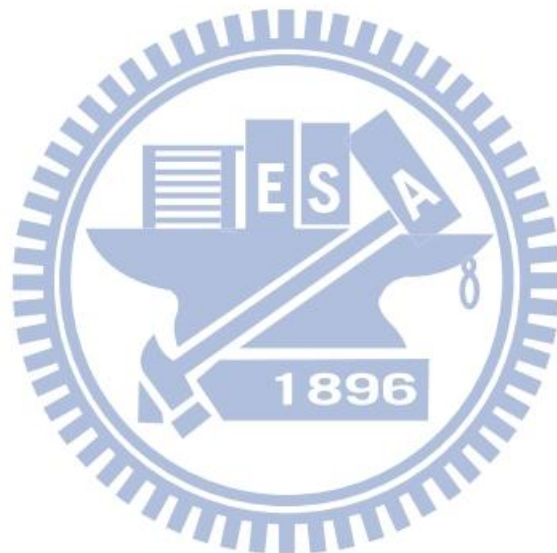
4. Laser-induced reduction of HAuCl$_4$ and AgNO$_3$ in solution

The HAuCl$_4$ solution was prepared from diluting 100 mM aqueous HAuCl$_4$ solution. The solution volume was 2 ml and extra 0.1 ml 1-propanol was added. The HAuCl$_4$ solution was irradiated by femtosecond laser through 10X objective lens in the range of energy from 0.3 to 40 µJ/pulse for 180 min. The focal position was adjusted at the center of a quartz cell in the height of 5 mm from bottom. The extinction spectra were measured before laser irradiation and at the irradiation time of 5, 10, 20, 30, 60, 90, 120, and 180 min. The Δextinction was calculated as subtraction between the laser exposed spectrum and the ion solution spectrum. The figure of Δextinction at 540 nm versus irradiation time was utilized since gold nanoparticles possess strong absorption and scattering around this wavelength. The peak wavelength was selected at the maximum Δextinction value (peak) around 500 nm to 600 nm. The figure of peak wavelength versus irradiation time demonstrates the particle size change on the basis of nanoparticle size dependence with absorption band.

The color of HAuCl$_4$ solution is pale yellow. While laser focuses into the solution, a series of bubbles are generated from the focal point and the color converts to red

after a period of irradiation. The figures of HAuCl$_4$ solution before and after femtosecond laser irradiation are shown in Fig. 4.1. It is known that the gold nanoparticles are generated since the extinction of gold nanoparticles is approximately located at 540 nm, which makes solution show red. Further irradiation causes the color become deeply.
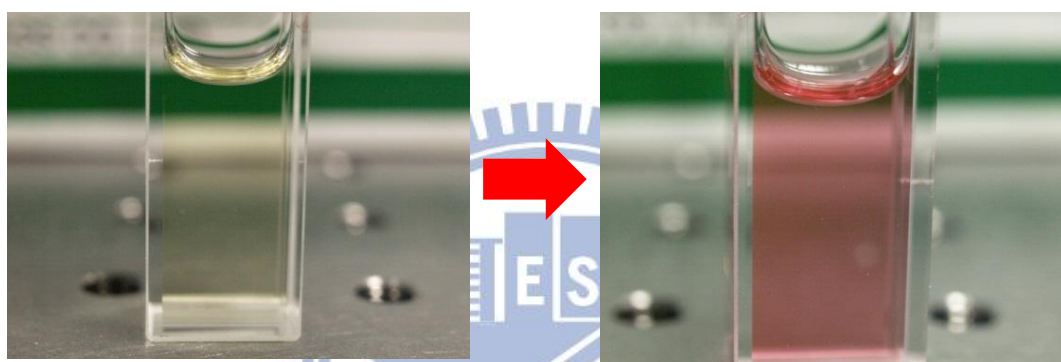
Fig.4.1 The pictures of HAuCl$_4$ solution before (left) and after (right) femtosecond laser irradiation.

4.1 HAuCl$_4$ concentration dependence of gold nanoparticle preparation

The HAuCl$_4$ solution was prepared from diluting 100 mM aqueous HAuCl$_4$ solution and extra 0.1 ml 1-propanol was added. The three different concentration HAuCl$_4$ solutions (0.5, 1, and 2 mM) were irradiated by femtosecond laser through 10X objective lens at 20 μJ/pulse for 180 min. The extinction spectra were measured

before laser irradiation and at the irradiation time of 5, 10, 20, 30, 60, 90, 120, and

180 min.

The Δextinction enhancement at 540 nm versus irradiation time in 2 mM HAuCl$_4$

solution is lower than that in 0.5 mM and 1 mM HAuCl$_4$ solution as shown in Fig. 4.2.

The obtained gold nanoparticles under the condition of 2 mM are much easy to

aggregate rather than the nanoparticles in 0.5 mM and 1 mM, which are examined by

SEM images.
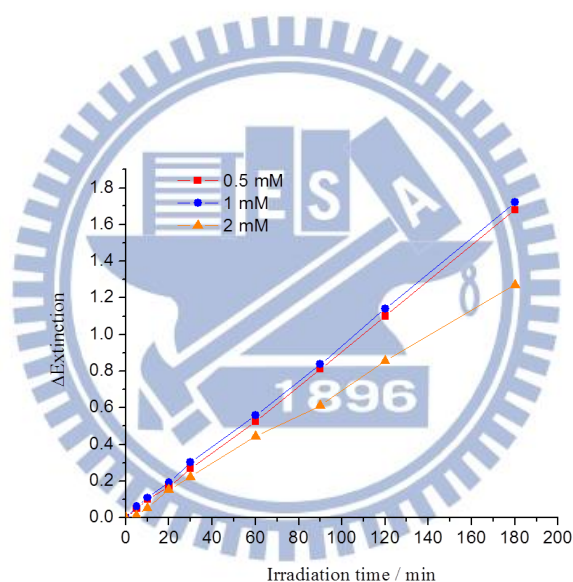
Fig.4.2 The Δextinction at 540 nm shows linear increase versus irradiation
time in 0.5, 1, and 2 mM HAuCl$_4$ solutions.

The figure of peak wavelength versus irradiation time is shown in Fig. 4.3. The

peak wavelength initially shifts to shorter wavelength within 30 min and then keeps at

constant wavelength. Finally the peak shifts to longer wavelength gradually owing to

the high concentration of gold nanoparticles. The formation of large nanoparticles in

high concentration becomes prominent due to nanoparticle growth and aggregation. However, the peak wavelength in 2 mM $HAuCl_4$ solution shifting to longer wavelength drastically after 30 min irradiation exceeds other two concentrations. This indicates that gold nanoparticle aggregation and particle growth are the main path in 2 mM $HAuCl_4$ solution after 30 min irradiation. The SEM images taken in 2 mM $HAuCl_4$ solution demonstrate wide particle distribution and large average size. On the other hand, large nanoparticles can scatter and absorb more light strongly, thus the Δextinction ought to be enhanced massively due to the influence of aggregation and particle growth. Nevertheless, large nanoparticles fabricated in 2 mM $HAuCl_4$ solution never reflect the deserved enhancement of Δextinction, indicating the fabrication in 2 mM $HAuCl_4$ solution is relatively inefficient.
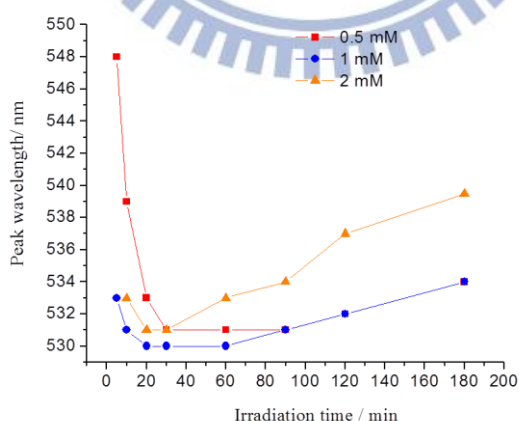
Fig.4.3 The peak wavelength versus irradiation in 0.5, 1, and 2 mM $HAuCl_4$ solutions. The nanoparticle size changes with the evolution of irradiation time.

4.2 Laser energy dependence of gold nanoparticle

preparation

0.5 mM HAuCl$_4$ solutions with the addition of 1-propanol were irradiated for 180 min at 5, 10, and 40 μJ/pulse individually. The corresponding condition is that 0.5 mM HAuCl$_4$ solutions without1-propanol were irradiated for 180 min at 5, 10, and 40 μJ/pulse individually. The Δextinction versus wavelength at the three pulse energies are shown in Fig. 4.4. We find the enhancement of Δextinction is dependent on the laser pulse energy. The Δextinction at higher laser energy increases quickly and obviously.
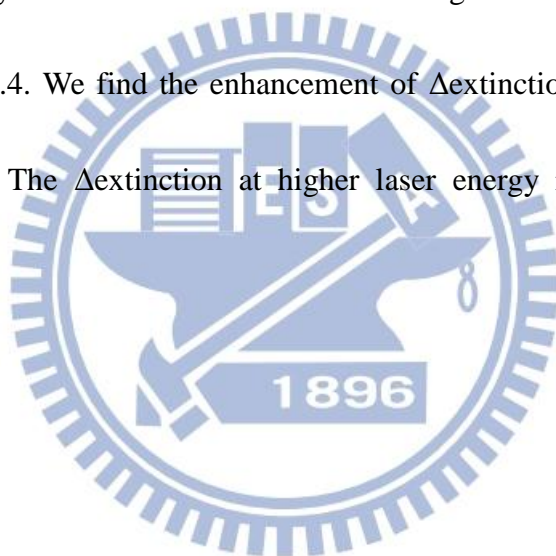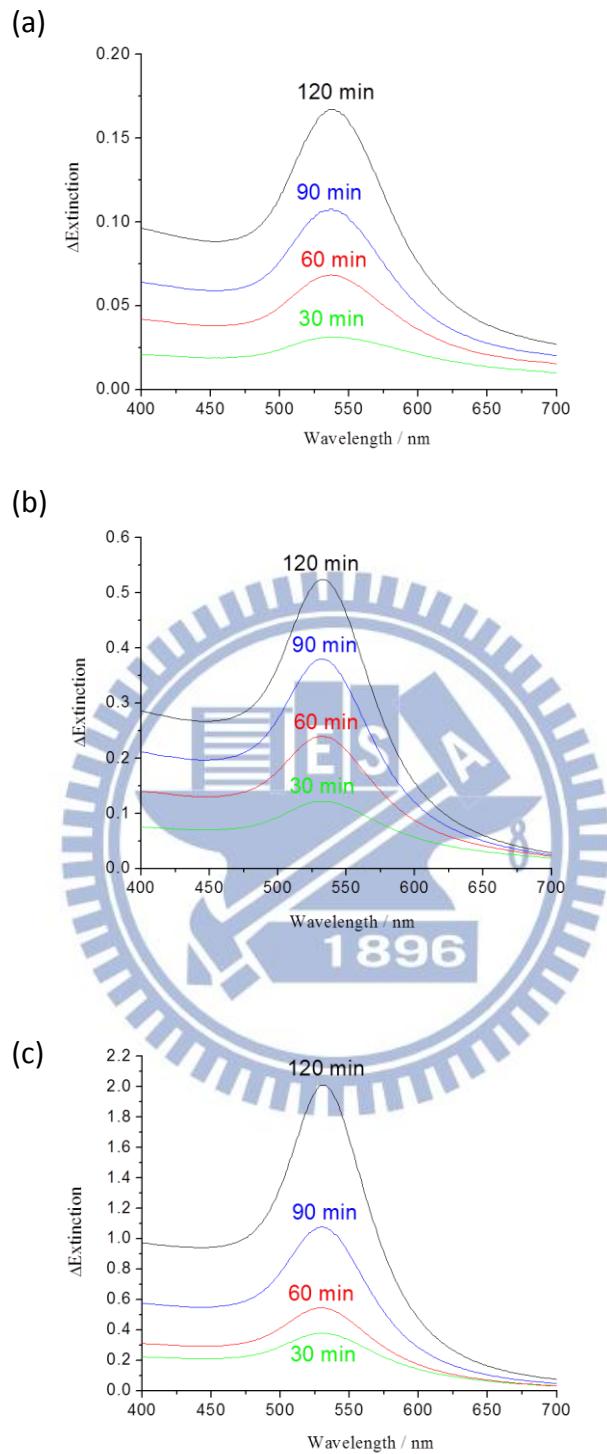
Fig.4.4 The Δextinction increases with the irradiation time at the pulse energy; (a) 5 µJ/pulse, (b) 10 µJ/pulse, and (c) 40 µJ/pulse. Rapid increase in the Δextinction is observed at higher energy.

Fig 4.5 shows that the Δextinction around 540 nm in the presence/absence of 1-propanol at the pulse energy; 5, 10, and 40 μJ/pulse. At 5 μJ/pulse, the Δextinction at 540 nm maintains zero in the absence of 1-propanol for 180 min irradiation but increases linearly in the presence of 1-propanol. The color of solution in the absence of 1-propanol is as same as the original solution. At 10 μJ/pulse, despite the Δextinction at 540 nm in the absence of 1-propanol initially maintains zero, long time irradiation still triggers the enhancement of Δextinction. After 150 min irradiation, the Δextinction starts to increase slightly. At 40 μJ/pulse, it takes 20 min at least to form gold nanoparticles in the absence of 1-propanol. No matter the HAuCl$_4$ solution involves 1-propanol or not, both spectra illustrate convex curve in the evolution of long time irradiation due to the extinction saturation. Numerous gold ions are reduced to gold nanoparticles and less gold ions are left in the solution, so the reduction rate begins to decline step by step. As a result, the reduction cannot support the enhancement of Δextinction and laser ablation becomes a dominant process, which leads to particle size reduction. The decline of Δextinction after saturation attributes to a high proportion of small nanoparticles which provide less extinction intensity.
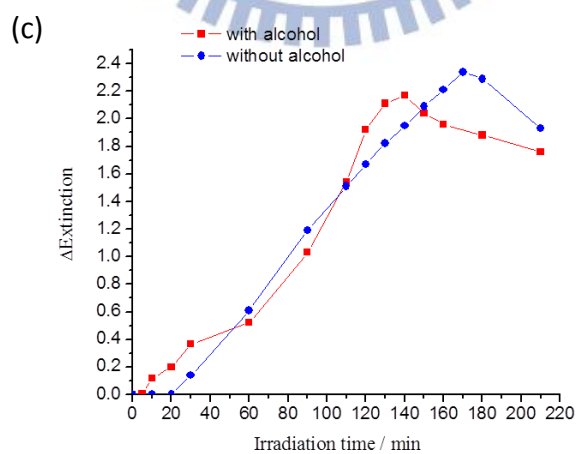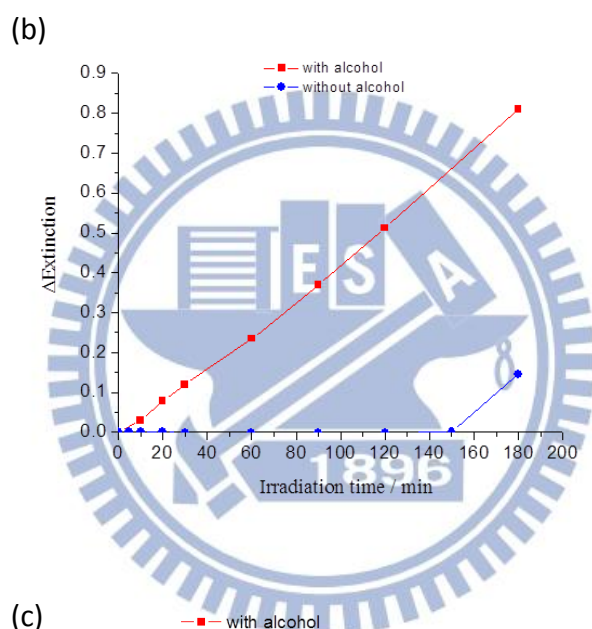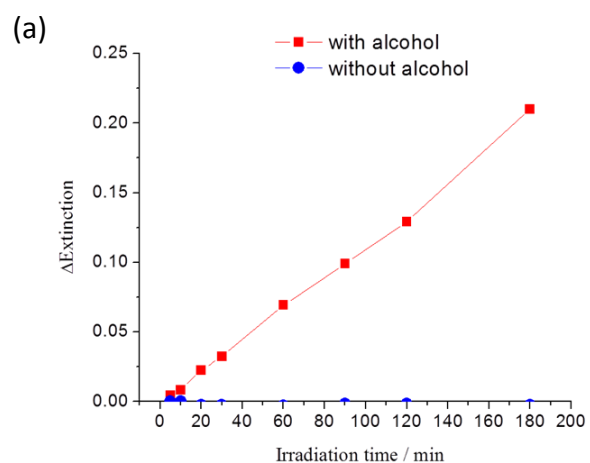
Fig.4.5 The Δextinction around 540 nm in the presence/absence of 1-propanol increases with the irradiation time at the pulse energy of (a) 5 μJ/pulse, (b) 10 μJ/pulse, and (c) 40 μJ/pulse.

0.5 mM HAuCl$_4$ solutions with the addition of 1-propanol were irradiated for 180 min at 0.3, 5, 10, and 20 μJ/pulse individually. Fig. 4.6 shows the Δextinction versus irradiation time at 540 nm among 4 pulse energies. Except the experiment at 0.3 μJ/pulse, the Δextinction at 540 nm increases linearly among the three different energies and illustrates the laser energy dependence. The energy threshold of cavitation bubble generation for the mixture of aqueous HAuCl$_4$ solution with 1-propanol is roughly 0.4 μJ/pulse. Below 0.4 μJ/pulse, no any secondary bubble can be observed via 10X objective lens and CCD camera. The Δextinction around 540 nm at 0.3 μJ/pulse seems to approach to zero, but actually a little of enhancement (~0.006) can be observed after 180 min irradiation, even though the energy (0.3 μJ/pulse) is lower than threshold of cavitation bubble generation. It is depicted that gold nanoparticles fabrication is able to be done without cavitation bubble generation. Such low energy still enables to trigger the reduction of gold nanoparticles, which urges us to consider the reduction mechanism without the cavitation bubble collapse-induced radicals.
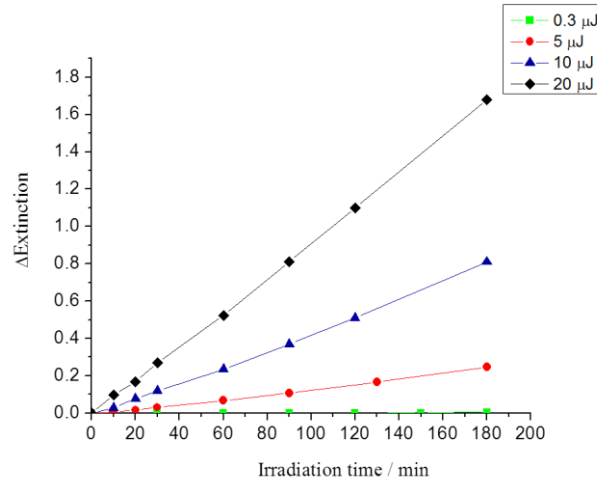
Fig.4.6 The Δextinction increase at 540 nm with irradiation time shows energy dependence.

Fig. 4.7 illustrates the peak wavelength against irradiation time among three energies. No peak wavelength can be found accurately at 0.3 μJ/pulse. All the three curves have a similar concave tendency and can be divided to 3 sections according to the progress of peak wavelength shifting. Firstly, the initial peak wavelength appears at long wavelength after sample exposes to laser for 5 to 10 min. The initial peak wavelength shifts to shorter wavelength drastically within 30 min irradiation. Secondly, the peak wavelength keeps at constant wavelength during 30 to 90 min irradiation. It means that the average size of gold nanoparticles in this period is the same approximately. Finally, the peak wavelength shifts to longer wavelength slightly after 90 min irradiation. In this section, the gold nanoparticle concentration is so high that aggregation and particle growth takes place apparently. In addition, the laser energy plays an important role on the affection of peak wavelength shift. The

magnitude of laser energy can decide the gold nanoparticle size and size distribution

because of laser ablation. Small gold nanoparticles are obtained at high laser energy

and vice versa. Hence, laser energy is an indispensable parameter on particle size

selection and an important physical phenomenon.
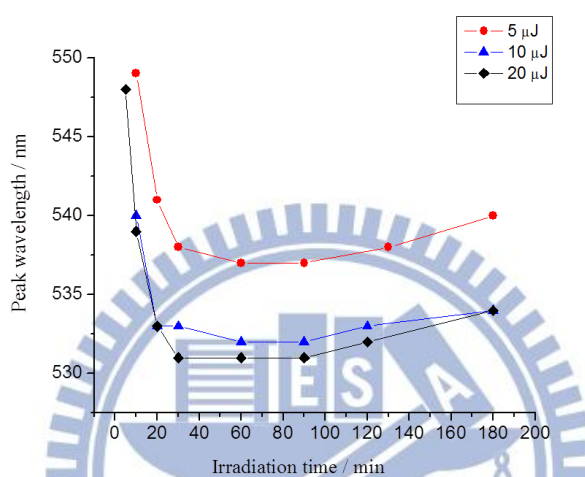
Fig.4.7 The relation between peak wavelength and irradiation time depends on the
laser energy. Larger nanoparticles are obtained at lower energy.

The Δextinction at 540 nm versus energy is shown in Fig. 4.8. The irradiation time

in each energy from 1 to 12 μJ/pulse is 30 min. The points plotted nonlinearly imply

that gold nanoparticle fabrication is based on nonlinear optical phenomena. The fitting

curve is second order equation, which strongly supports the assumption of two

photons absorption of $HAuCl_4$ solution.
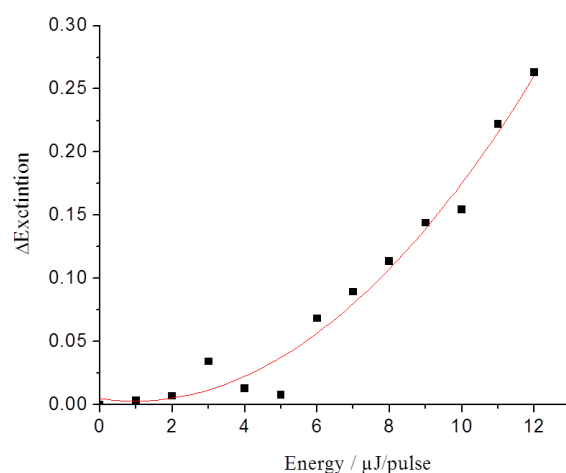
Fig.4.8 The Δextinction at 540 nm versus laser pulse energy. The fitting curve is based on 2nd order equation.

4.3 Irradiation time dependence of gold nanoparticle

preparation

0.5 mM HAuCl$_4$ solution with the addition of 1-propanol was irradiated for 210 min at 40 μJ/pulse. The peak wavelength against irradiation time was recorded and shown in Fig. 4.9. The initial peak wavelength appears at long wavelength and shifts to shorter wavelength drastically within 60 min irradiation. Then, the peak wavelength shifts to longer wavelength slightly after 60 min irradiation. The solution achieves saturated at 130 min approximately and then the peak wavelength starts to decline. We suppose that the initial peak wavelength shifting to shorter wavelength indicates the gold nanoparticle size decreases in the beginning reduction. The initial

particle size is quite large due to localized high concentration of nanoparticles or atoms around focal point. The high dense atoms or nanoparticles in a tiny volume cause particle aggregation and growth severely. This size reduction process can be described by laser ablation which changes the particle structure over time. The peak wavelength shifting toward longer wavelength until 110 min is due to particle growth and aggregation in the environment of high gold nanoparticle concentration. As the course of irradiation, the gold ions in solution are exhausted gradually and fewer ions exist in the ultimate process. While the formed gold atoms cannot be supplied to further aggregate as a particle rapidly in the solution, the competitive process, laser ablation on gold nanoparticles becomes dominant and leads to size reduction.

The SEM images and size distribution diagrams shown in Fig. 4.10 can coincide with the figure of peak wavelength against irradiation time as shown in Fig. 4.9. At least 120 particles in each condition were estimated and then we could plot diagrams and calculate the average size. Fig. 4.10 (a1) and (a2) are SEM images taken on 10 min irradiation at 40 μJ/pulse. Fig. 4.10 (b1), (c1), and (d1) are SEM images taken on 60, 120, and 180 min irradiation and the corresponding size distribution diagrams are seen in Fig. 4.10 (b2), (c2), and (d2). Fig. (a1) and (a2) show that large and small nanoparticles coexist in the beginning of irradiation, demonstrating aggregation and small single nanoparticle formation take place simultaneously. Fig. 4.10 (b2) shows

gold nanoparticle distribution and the average size is 32 nm. The size distribution of

gold nanoparticles by 120 min irradiation is shown in Fig. 4.10 (c2). The average size

is 37 nm and the particle size shifts to both sides, forming double peaks; some

particles become smaller, others become larger. Fig. 4.10 (d2) shows that size

distribution tends to concentrate on small scale and gold nanoparticles average size is

15 nm. These SEM images and size distribution diagrams precisely provide the direct

view on particles shape and association to spectra.
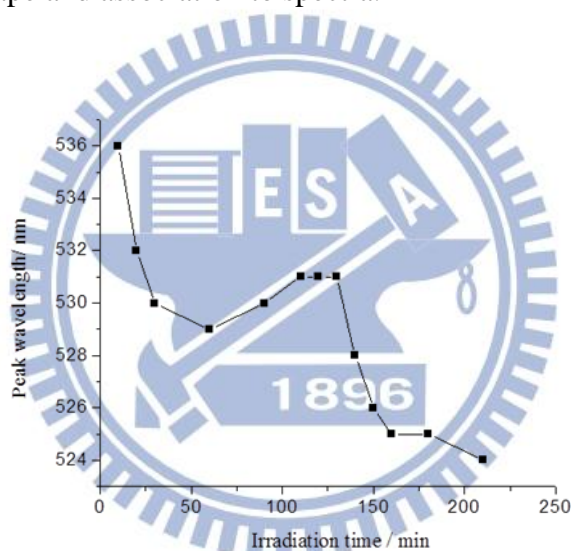
Fig.4.9 The peak wavelength against irradiation time at 40 μJ/pulse. The nanoparticle size varies with irradiation time.
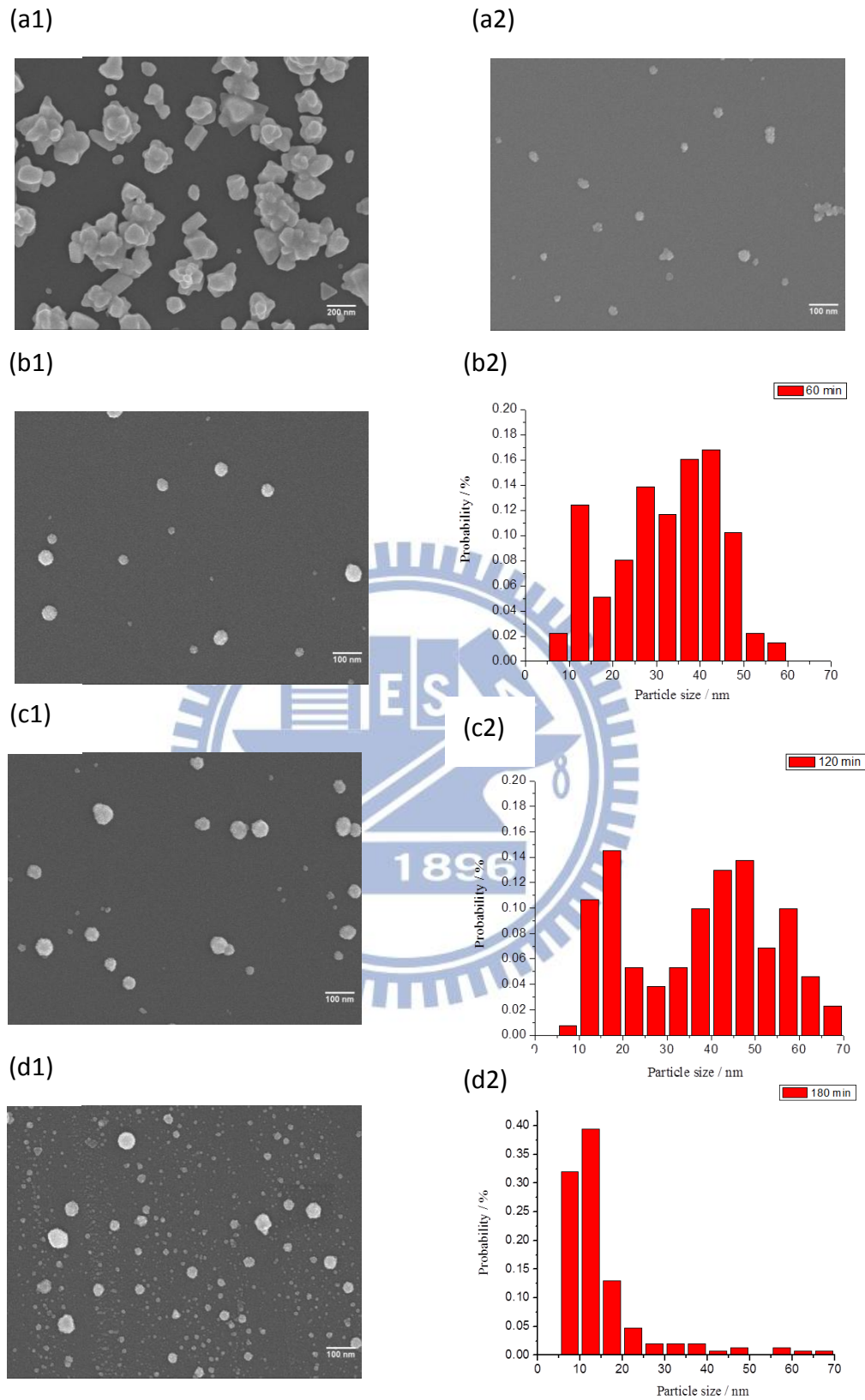
Fig.4.10 SEM images taken at the irradiation time of (a1) & (a2) 10 min, (b1) 60 min, (c1) 120 min, and (d1) 180 min. (b2), (c2), and (d2) are the size distribution estimated from the corresponding SEM images of (b1), (c1), and (d1).

4.4 AgNO$_3$ and Polyvinylpyrrolidone (PVP) concentration

dependences of silver nanoparticle preparation

100 mM AgNO$_3$ aqueous solution was mixed in polyvinylpyrrolidone (PVP) solution. The concentration of AgNO$_3$ and PVP is 1 mM and 10 mg/ml respectively. The preparation of the sample in the presence of 1-propanol was that 100 mM AgNO$_3$ solution diluted to 1 mM AgNO$_3$ solution of 2 ml and extra 0.1 ml 1-propanol was added. The sample in the absence of PVP and 1-propanol was 1 mM AgNO$_3$ solution. The pulse energy was set at 40 μJ/pulse and the irradiation time was 180 min. The figure of Δextinction versus irradiation time at 425 nm was utilized since silver nanoparticles possess strong absorption and scattering in this wavelength.

We observe that the Δextinction at 425 nm rises only in the presence of PVP as shown in Fig. 4.11. Fig. 4.12 illustrates that the color of AgNO$_3$ solution in the presence of PVP changes from transparent to orange and the preparation of silver nanoparticles is quite efficient on the basis of extinction spectra. The color is unchanged in the both cases while the sample solutions are in the absence of PVP. However, the spectra demonstrate a little enhancement around 425 nm (~0.02) after 180 min irradiation, indicating silver nanoparticles are fabricated exactly. But, the production yield of silver nanoparticles without any chemicals is quite low, indicating

silver nanoparticle fabrication in the absence of PVP is inefficient. Hence, PVP is decided to involve in the reduction and we will discuss the role of PVP in the sequent experiments.
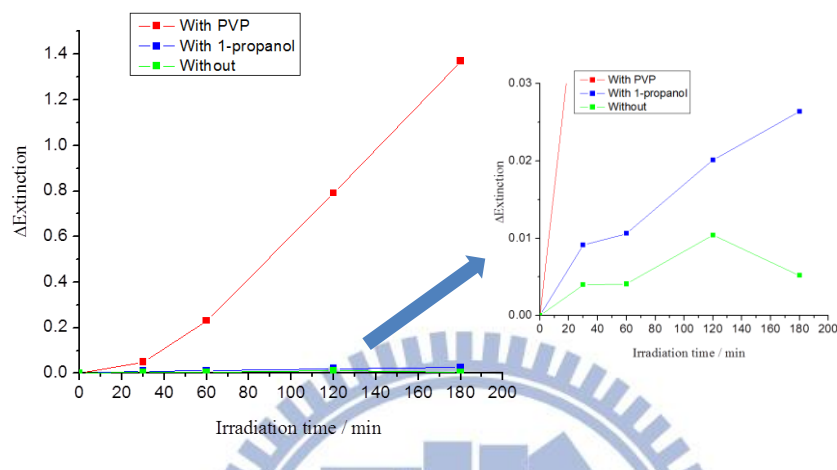
Fig.4.11 The Δextinction of $AgNO_3$ solution at 425 nm versus irradiation time under the three conditions; with PVP, with 1-propanol, and without any chemicals. A large extinction change was found in the presence of PVP.
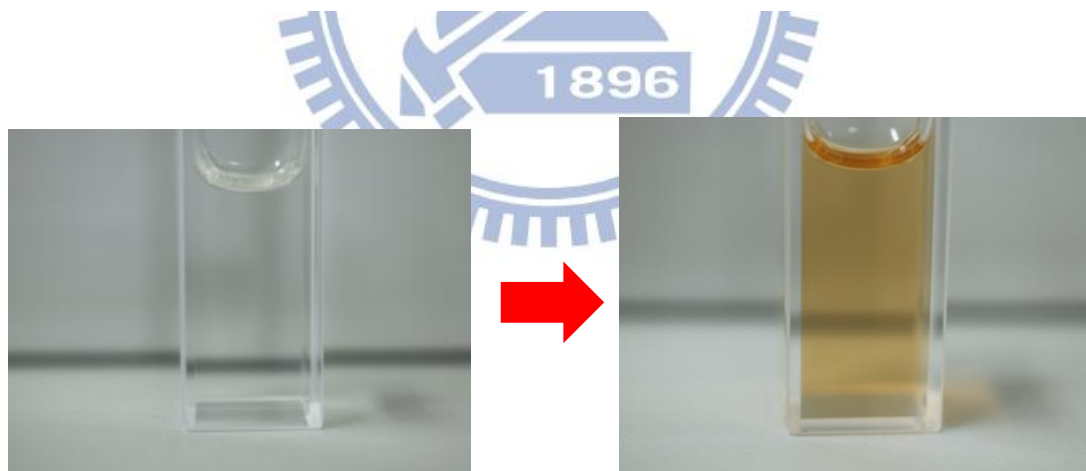
Fig.4.12 The pictures of $AgNO_3$ solution before (left) and after (right) femtosecond laser irradiation.

AgNO$_3$ aqueous solution was mixed in 20 mg/ml PVP solution and the concentration of AgNO$_3$ is adjusted to 0.25, 0.5, and 1 mM respectively. Fig. 4.13 shows Δextinction at 425 nm versus irradiation time among three AgNO$_3$ concentrations at 40 μJ/pulse. It is obviously demonstrated that silver nanoparticles fabrication is proportional to AgNO$_3$ concentration. The factor of particle size which may influence the extinction intensity can be excluded because the curves of peak wavelength among different AgNO$_3$ concentration are not consistent with Δextinction enhancement at 425 nm. We can directly regard Δextinction enhancement at 425 nm as the contribution of silver nanoparticles concentration. Much more silver nanoparticles are obtained in higher concentration of AgNO$_3$ solution, which presents AgNO$_3$ concentration dependence.
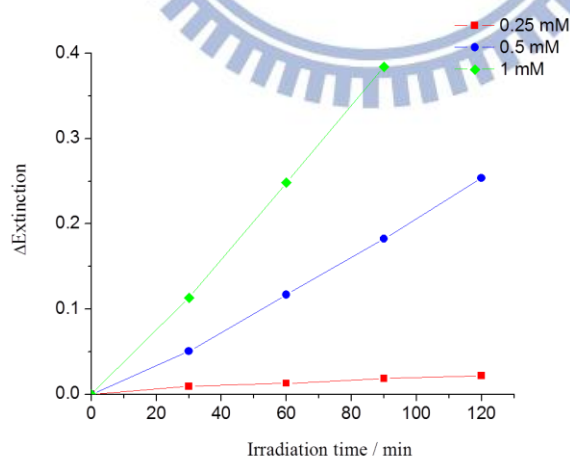
Fig.4.13 The Δextinction at 425 nm versus irradiation time among 0.25, 0.5, 1 mM AgNO$_3$ concentration at 40 μJ/pulse. AgNO$_3$ concentration dependence is observed.

1 mM AgNO$_3$ aqueous solution was mixed in 2, 5, 10, and 20 mg/ml PVP

solution respectively. The molar ratio of PVP/ AgNO$_3$ is 0.2, 0.5, 1, and 2. The pulse

energy was set at 40 μJ/pulse and the irradiation time is 180 min.

Fig. 4.14 shows Δextinction at 425 nm versus irradiation time among four

concentration of PVP. The Δextinction at 425 nm enhancement accompanies with the

irradiation time and expresses positive correlation to PVP concentration. More silver

nanoparticles are obtained in higher PVP concentration[29].
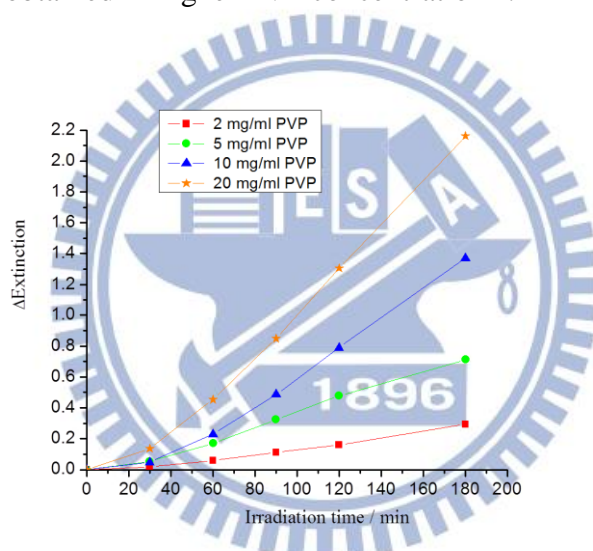
Fig.4.14 The Δextinction at 425 nm versus irradiation time among four concentration of PVP. The yield of silver nanoparticles depends on PVP concentration.

4.5 Discussion

4.5.1 Laser energy dependence of gold nanoparticle

preparation efficiency and bubbling threshold

The amount of reduced gold nanoparticles is dependent on the laser energy, which is confirmed directly from laser energy dependence experiment. The concentration of reduced atoms ought to be correlated to the photon intensity. On the other hand, the $HAuCl_4$ solution with 1-propanol possesses efficient optical reduction, which implies that 1-propanol involves the reduction or acts as a stabilizer despite 1-propanol cannot reduce gold ion directly without laser irradiation. The gold nanoparticle fabrication in the presence of 1-propanol at low laser energy exhibits an apparent distinction compared to that in the absence of 1-propanol. It is inefficient that the fabrication in the absence of 1-propanol at low laser energy, which is illustrated in Fig. 4.5 (a) and (b). However, the distinction becomes close while the laser energy is gradual rising. The increasing pulse energy shortens the incubation time in which gold atoms aggregate to nanoparticles. Gold atom concentration is not high enough to aggregate as a nanoparticle during incubation so no extinction signal can be measured. It means that reduction occurs sequentially during laser irradiation even without the addition of 1-propanol.

For long irradiation time, the saturated solution can be achieved while we observe that the Δextinction is climaxed. At this time, the reduction rate of gold nanoparticles is nearly equal to the laser ablation rate of gold nanoparticles. The reduction rate starts to slow down because the concentration of gold ions is not enough to support further reduction. High percentage of gold ions has already converted to gold nanoparticles and meanwhile, laser ablation becomes the dominant path. We can suppose that the competition between reduction and ablation which exists simultaneously guides to the investigation of controlled nanoparticle size.

So, laser ablation continues working on the nanoparticles and its magnitude is determined by the pulse energy. It is the evidence that the location of the peak wavelength is according to the magnitude of pulse energy, indicating the strength of laser ablation influences the nanoparticle size. Large nanoparticles may prior to be ablated owing to high absorption for long diameter nanoparticles. Therefore, the average size of nanoparticles declines with the increase of pulse energy.

Indeed, gold nanoparticle fabrication above bubbling threshold is observed exactly. When the pulse energy is 0.3 μJ/pulse lower than bubbling threshold (0.4 μJ/pulse approximately) for the sample solution, eventually a little of enhancement (~0.006) around 540 nm can be observed after 180 min irradiation, indicating gold nanoparticles fabrication still occurs without any bubbles generation. The reduction of

gold nanoparticles by radicals generated during cavitation bubble collapse is published in sonochemistry.

4.5.2 Irradiation time dependence of gold nanoparticle size

We find that the peak wavelength is not constant but variable with the progress of irradiation time. We must consider two reasons together in the meantime; laser ablation, and aggregation or particle growth. Laser ablation working on nanoparticles persists till the end of laser irradiation and it relates to particle size intensely. The constitution of smaller nanoparticles increases with irradiation time. One obvious particle size reduction is observed after the solution achieves saturated. The size distribution becomes narrow and tends to small size apparently due to the fragmentation of large nanoparticles. The procedure can be regarded as the top-down method which is analog to fabrication of nanoparticles by laser ablation.

The total surface free energy in the solution is fixed at constant and the surface free energy of each particle is not proportional to its particle size. While the particle concentration of colloidal solution achieves the critical condition, the decrease of total surface free energy as a driving force reverses to the equilibrium state toward large particle development. The frequent collision of particles causes aggregation which drastically increases particle size and decreases total surface free energy. Meanwhile,

the consideration of particle growth is essential and the process of particle growth is unidentified to aggregation. The gold atoms adhere on the surface of gold nanoparticles and then combine together as one during particle growth. Both these two factors can increase particle size and shift peak wavelength to longer wavelength.

In the beginning of fabrication, a little volume $HAuCl_4$ is reduced around focal point and high concentration of gold atoms appears rapidly in a tiny space. The localized inhomogeneous concentration of gold nanoparticles causes severe aggregation, leading to the generation of large particles (diameter above 50 nm) and wide size distribution. Non-identical size nanoparticles coexist and diffuse gradually to surrounding during the fabrication. However, laser ablation on nanoparticles decreases the average particle size with the evolution of irradiation time until the equilibrium state of particle ablation, particle aggregation and particle growth. So, the initial peak wavelength which locates at longer wavelength is due to localized particle enlargement and the peak wavelength shifting to shorter wavelength is due to laser ablation. The size enlargement which is dominated by aggregation and particle growth competes with the size reduction which is controlled by laser ablation.

4.5.3 Concentration dependence of preparation yield

In gold nanoparticle fabrication, the production yield in different concentrations

of gold ion exhibits almost equalization at the same energy. However, the production

yield of silver nanoparticle is strongly dependent on ion concentration unlike the gold

nanoparticle yield only depends on the pulse energy[30]. The reduced ability of

femtosecond laser should be proportional to pulse energy and ion concentration

drastically. For gold nanoparticle preparation, we also attempted to fabricate gold

nanoparticles in much higher $HAuCl_4$ solution. The precipitation could be observed

even during laser irradiation, indicating few micrometer size gold particles were

generated because dense gold atoms or nanoparticles in a tiny volume aggregate as

forming quite large nanoparticles. Based on the result, the $HAuCl_4$ concentration

which is far below 0.5 mM is suggested to depend on pulse energy. Moreover, $AgNO_3$

is a kind of salt which can dissolve in solution as Ag^+ and NO_3^- completely. So, the

silver nanoparticle reduction associating to ion concentration shows that the

femtosecond laser induces reaction on silver ion indirectly because Ag^+ must be

reduced by other species. In addition, PVP concentration also affects the reduction

yield, indicating PVP plays a key point on reduction.

4.5.4 Preparation mechanism of gold and silver nanoparticle

First, we should discuss one-photon absorption at 800 nm of the fundamental

wavelength of femtosecond laser for each the compound we used in this experiment.

For $AuCl_4^-$, it was reported that the aqueous solution of $HAuCl_4$ shows only three absorption band at 217 nm, a shoulder at 287 nm, and 322 nm. The former two are ascribed to be the ligand-to-metal charge transfer (LMCT) bands of $AuCl_4^-$ between gold and chloro ligands[31]. The latter one at 322 nm directly originates from the d-d transition of the $AuCl_4^-$[32]. While, $AgNO_3$ is soluble in water dissociate into Ag^+ and NO_3^- ions, and no absorption owing to LMCT and d-d transition of $AgNO_3$ is expectable. For 1-propanol, this compound is made up of σ bonds. It is well known that the energy of σ to σ* electronic transition corresponds to an absorption of ultraviolet photon. For PVP, the electronic transition absorption of this compound can be considered as π-π* and n-π* transitions, which the details have been already identified. It was reported that the spectrum of PVP in H_2O shows only two electronic absorption bands with maxima at 270 and 440 nm, although the latter peak is not so clear in our study. The former intense band at 270 nm can be attributed to be the π-π* transitions of the conjugated double bond in PVP carbonyl group. As for the weak band that is detected in the visible region at 440 nm, it is attributed to the n-π* transitions of unbonding electrons of carbonyl oxygen[33]. Therefore, since it can be considered that all the compounds we used in this experiment have no one-photon absorption at 800 nm, these nanoparticles formation are attained through multiphoton absorption participates.

According to the results of the extinction spectrum of HAuCl$_4$, AuCl$_4^-$ aqueous solution surely has the absorption at 400 nm, so that simultaneous 2-photon excitation should be considered. Although a very high absorption in water at 200 nm, 2-photon absorption is much prominent process because of the large difference between two-order nonlinear susceptibility and four-order one. Assuming the Δextinction is proportional to energy intensity to N times, the plot of log (Δextinction) versus log (energy) shows the slope N of the linear fitting line as shown in Fig. 4.15. As a result, the slope N in our experiments is estimated to be 2.0 and 1.8 for two sets of experiments, which strongly indicates that the formation process occurs through 2-photon absorption by AuCl$_4^-$. This simplifies the inference of mechanism of gold nanoparticle fabrication since only AuCl$_4^-$ absorption directly relates to photon absorption-induced reaction. Considering our experimental results, we propose the reduction mechanisms of gold ion based on 2-photon process as follows;

$$\left\{ \begin{array}{l} AuCl_4^- \xrightarrow{2h\nu} Au^0 + Cl_2 + Cl^- + Cl\bullet \\ nAu^0 \rightarrow (Au)_n \end{array} \right.$$
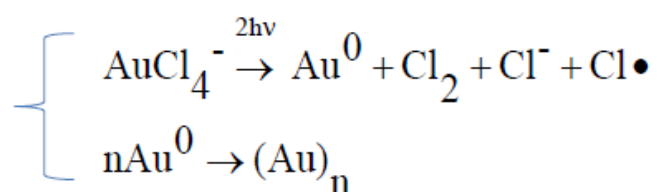
The AuCl$_4^-$ directly absorbs two photons simultaneously, and progress to gold atom, chloride, chloride ion, and chloride radical. The formed gold atoms then aggregate to each other, forming the large nanoparticle. The addition of 1-propanol in the solution can stabilize intermediate chloride radicals, which enhances this chemical

reaction and increases the reaction rate. Indeed, the addition of 1-propanol accelerates the formation of gold nanoparticle. Without 1-propanol, the precipitation are easily induced within few hours after the irradiation.
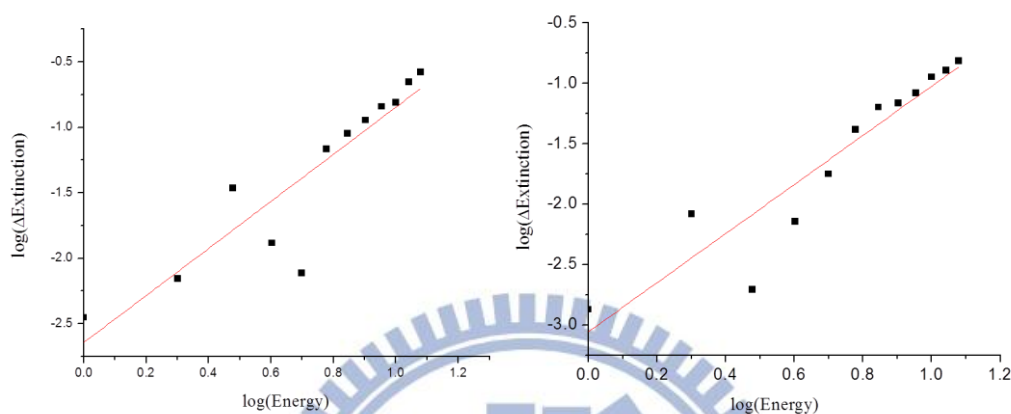
Fig.4.15 The plot of log(Δextinction) versus log(energy) depicts that the slope of linear fitting line is (a) 1.8 and (b) 2.0. HAuCl$_4$ concentration is (a) 0.5 mM and (b) 2 mM.

For silver nanoparticle fabrication, we can observe apparent change in extinction intensity only in the presence of PVP. This indicates PVP plays an important role in the reduction. Since the production of dissociation of AgNO$_3$, Ag$^+$ and NO$_3^-$, don't absorb visible light, PVP should be responsible for the main reduction based on 2-photon absorption. As described above, PVP has a sufficient absorption coefficient for 2-photon absorption. Therefore, PVP is firstly reacted, and one electron can be ejected from a lone pair electron on oxygen atom of PVP as below reaction formulas. This ejected electron owns a powerful reducing property and high negative standard electrode potential is offered to Ag$^+$ that is the electron acceptor, forming a zero

charge silver atom. In brief, the formation of silver nanoparticles takes place through 2-photon absorption of PVP[34]. Besides, PVP radical is always reversed to the initial PVP in the interaction with water, with keeping the amount of PVP maintain at constant. The reduction mechanism of silver nanoparticle is summarized below.

$$\begin{cases} \mathrm{AgNO_3 \rightarrow Ag^+ + NO_3^-} \\ \mathrm{PVP \overset{2h\nu}{\rightarrow} PVP\bullet + e^-} \\ \mathrm{Ag^+ + e^- \rightarrow Ag^0} \\ \mathrm{nAg^0 \rightarrow (Ag)_n} \end{cases}$$
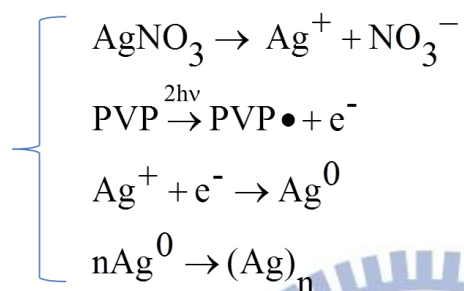
Note that a slight extinction intensity change is observed even without PVP in the solution, showing that a little of silver nanoparticles forms exactly. Since the solution has no PVP, it is absolutely transparent at 400 nm. Thus, we suggest that the silver nanoparticle fabrication may be caused by 4-photon absorption of water. For early studies on sonochemistry, it has been reported that hydroxyl radicals are generated during sonication in water[18, 35]. The reactive transient species such as hydrogen radicals, hydroxyl radicals, electrons and so on are essential to consider while multiphoton absorption of water takes place[30]. Hence, these reactive transient species are formed by femtosecond laser irradiation and enables to reduce metal ions through 4-photon absorption of water. The probable 4-photon mechanism is described below.

$$\text{Ionization}\ \text{(lower energy)} \Rightarrow \left[\begin{array}{l} H_2O + mh\nu \rightarrow H_2O^+ + e^- \\ H_2O^+ + H_2O \rightarrow H_3O^+ + {}^\bullet OH \\ H_3O^+ + e^- \rightarrow H_2O + {}^\bullet H \end{array} \right.$$

Above bubbling threshold

$$\text{Ionization} + \text{cavitation}\ \text{(higher energy)} \Rightarrow H_2O \rightarrow {}^\bullet H + {}^\bullet OH$$

(bubble collapse)
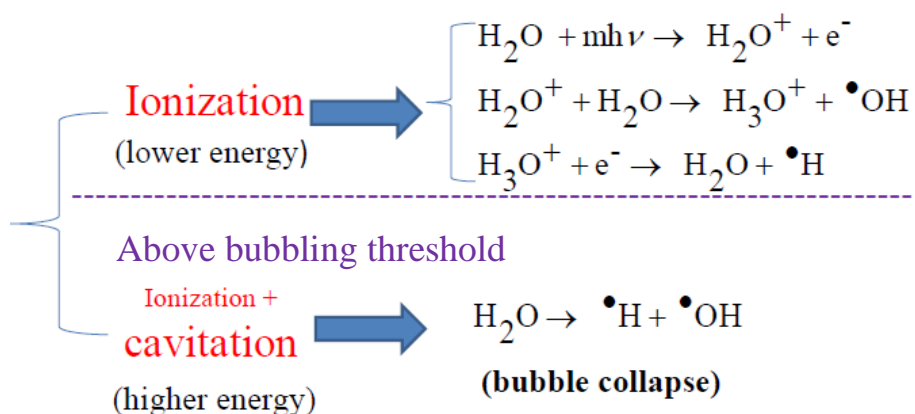
4-photon reduction process of water can be divided to 2 sessions according to the cavitation bubbling threshold of solution: irradiation-induced ionization and cavitation bubble generation. Femtosecond laser induced ionization is analog to gamma ray irradiation of aqueous solution at high energy where the transient species can be generated through water radiolysis. The complicated chemical reactions through ionization are summed up simply to the generation of high dense hydrogen radicals, hydroxyl radicals and electrons. Generally, the radiation-induced formation of metal nanoparticles in the reported papers is carried out under the condition of alcohol or ketone in metal ion solution, which can be a radical scavenger whose lifetime is much longer and reduction potential is higher[20-21]. This can explain that extinction intensity in the addition of 1-propanol is higher than that without any chemicals because of 1-propanol radicals. On the other hand, extremely high-temperature causes the formation of dense hydrogen and hydroxyl radicals during the cavitation bubble collapse. Both these two reactions are considered to be proposed in the view of

4-photon absorption of water. In conclusion, we proposed the reduction mechanisms

based on 2-photon absorption of $AuCl_4^-$ and PVP as well as 4-photon absorption of

water.

4.6. Surfactant effects on the preparation process

4.6.1 Polyvinylpyrrolidone (PVP) effect on gold nanoparticle

preparation

0.5 mM $HAuCl_4$ mixed in 20 mg/ml PVP solution with the addition of

1-propanol were irradiated for 150 min at 40 μJ/pulse. After stopping laser irradiation,

we kept the solution in dark environment at room temperature and measured the

spectra each day until 5 days later. The gold nanoparticles preserved for 5 days were

taken by SEM measurement. The size distribution and average size could be

estimated over 120 particles from SEM images.

Fig. 4.16 illustrates the Δextinction at 540 nm and peak wavelength versus time

in 5 days. Both the Δextinction at 540 nm and peak wavelength present a rise

tendency within 2 days and then a constant state after 2 days. The Δextinction at 540

nm increasing slightly within 2 days is corresponding to the shifting of peak

wavelength, indicating gold nanoparticles continue to grow up or aggregate. During 2

and 5 days, the gold nanoparticles in the solution remain homogenous and stable. Few aggregate in 5 days later can be observed from SEM images as shown in Fig. 4.17 and size distribution diagram of gold nanoparticles demonstrates narrow size distribution. The average size is 18 nm. Several days later, no any precipitant can be found and gold nanoparticles in the solution preserve homogenous dispersion. Analysis of spectra and SEM images shows that PVP can stabilize gold nanoparticles for long time and diminish particle growth and aggregation as a result of formation of narrow size distribution.

The Δextinction at 540 nm increases in three conditions, with PVP, with 1-propanol, and without any chemicals as shown in Fig. 4.18. Gold nanoparticles are fabricated in these three conditions exactly and the preparation becomes relative efficient in the presence of PVP slightly contrast with other conditions. But, the Δextinction with PVP achieves saturated within 70 min, which is faster than that with 1-propanol and without any chemicals. This can be discussed in the view of competition of $AuCl_4^-$ and PVP for absorption of photons.
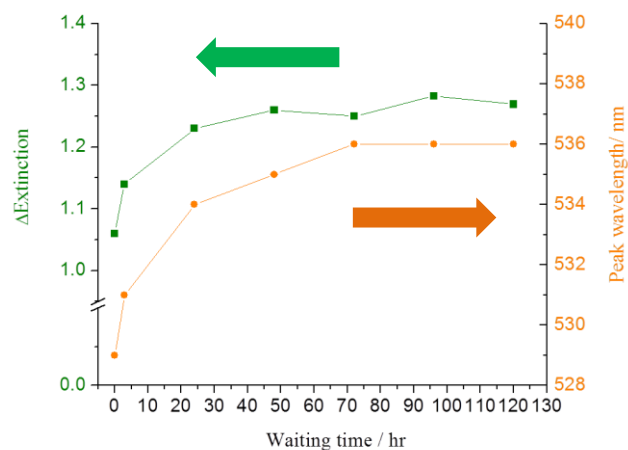
Fig. 4.16 The Δextinction at 540 nm versus the waiting time and the peak wavelength versus the waiting time in 5 days. Some changes of the peak wavelength and the Δextinction are recorded within two days. Gold nanoparticles keep their size after 2 days.
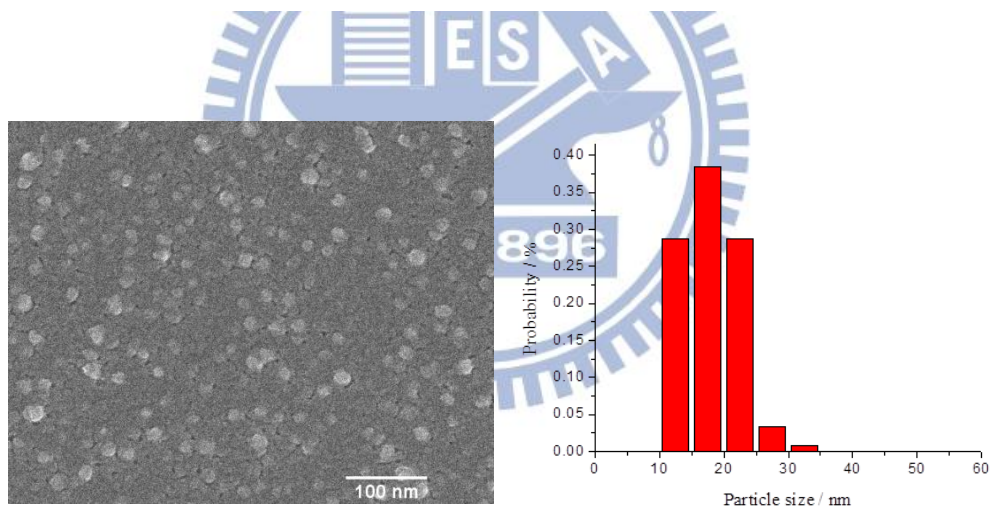
Fig. 4.17 The SEM image and size distribution diagram of gold nanoparticles after keeping 5 days. The size distribution is narrower with than without PVP and few aggregates are observed.
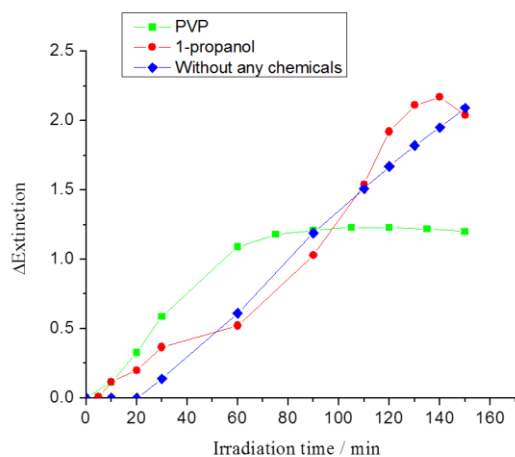
Fig. 4.18 The Δextinction at 540 nm increases under three conditions; with PVP, with 1-propanol, and without any chemicals. The solution with PVP becomes saturated in short time.

4.6.2 Polyvinylpyrrolidone (PVP) effect on silver nanoparticle preparation

1 mM AgNO₃ aqueous solution was mixed in 2, 5, 10, and 20 mg/ml PVP solution respectively. The molar ratio of PVP/ AgNO₃ is 0.2, 0.5, 1, and 2. The pulse energy was set at 40 μJ/pulse and the irradiation time is 180 min.

The peak wavelength against irradiation time among four concentration of PVP is shown in Fig. 4.19. All the experiments under four conditions point out the peak wavelength decline with irradiation time. Except the beginning of the experiment in 20 mg/ml PVP, the peak wavelength is dependent on the concentration of PVP. High concentration of PVP tends toward longer wavelength, meaning the formation of

larger nanoparticles. However, the peak wavelength in 20 mg/ml PVP within 60 min irradiation is shorter than that in 10 mg/ml PVP but the Δextinction at 425 nm in 20 mg/ml PVP is obviously higher than that in 10 mg/ml PVP. It depicts that the concentration of silver nanoparticles is the dominant reason in the enhancement of Δextinction not the effect of particle size. The effect of particle size is inferior factor which affects Δextinction in comparison with superior factor of particle concentration. The fabrication rate can be mainly ascribed to the concentration of PVP.

Fig. 4.20 is the SEM images taken in 30 min irradiation. It is clear that more aggregate can be found in high molar ratio of PVP/AgNO$_3$. The concentration of silver nanoparticles and the effect of molar ratio of PVP/AgNO$_3$ must be considered simultaneously. In short, the silver nanoparticle fabrication in high molar ratio of PVP/AgNO$_3$ expresses rapid formation rate and more aggregate generation.
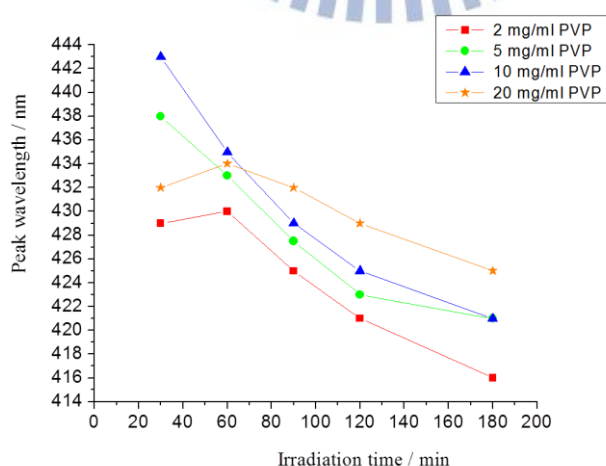

Fig. 4.19 The peak wavelength against irradiation time for four concentration of PVP. The peak wavelength declines with irradiation time and depends on PVP concentration.
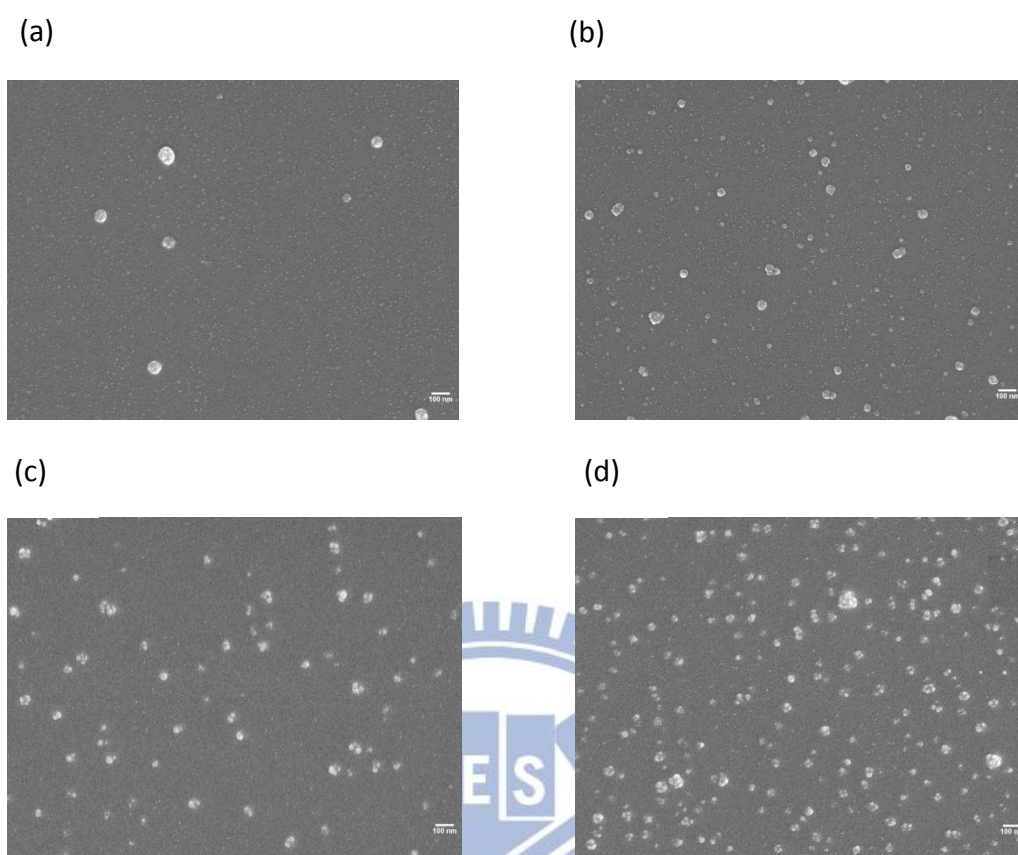
Fig. 4.20 SEM images taken with different molar ratio of PVP/AgNO$_3$; (a) 0.2, (b) 0.5, (c) 1, and (d) 2. The irradiation time is 30 min and pulse energy is 40 μJ/pulse.

4.7. Discussion

The gold nanoparticles in the presence of PVP dispersing homogenously in solution are relatively stable and can be kept for a long time without the following aggregation and precipitation. It can be discussed in view of PVP protection on the surface of gold nanoparticles. The nitrogen or oxygen atom of PVP can interact to the gold atom, forming a layer on the surface[29, 36]. The PVP layer coating on gold nanoparticles resists the collision and keeps the nanoparticles away from each other. Fig. 4.21 demonstrates one PVP layer coating on the surface of silver nanoparticles. We believe that PVP on nanoparticles prevents further aggregation and particle growth, and disperses the nanoparticles well as a homogenous colloidal solution. Meanwhile, the narrow size distribution and small size of nanoparticles can be obtained in the presence of PVP[9e, 30]. Generally, the gold nanoparticles in a close size distribution can be stored for a period.

Besides, 2-photon absorption of $AuCl_4^-$ and PVP are the competition process. When $AuCl_4^-$ concentration dilutes during the sequential reduction until the percentage of $AuCl_4^-$ is low, 2-photon absorption of PVP becomes prominent. The PVP radicals and electrons obtained from PVP dissociation cannot reduce negative charge $AuCl_4^-$. Consequently, High percentage of PVP hinders the further reduction, resulting in solution achieves saturated. In summary, the role of PVP in the process of

gold nanoparticles preparation mainly acts as surfactant and competitor of photon absorption with $AuCl_4^-$.

It is worthy to be note that the peak wavelength declines with the progress of irradiation both in gold and silver nanoparticle fabrication while PVP involves in solution. Laser ablation takes place on nanoparticles and makes them shrink on particle size in that further aggregation and particle growth are prohibited by PVP coating layer. Nanoparticles tend to develop with smaller size through laser irradiation.

However, more aggregates and larger size nanoparticles can be observed at high molar ratio of $PVP/AgNO_3$, attributing to localized high concentration of atoms or nanoparticles around focal point. High dense silver atoms confined in a small space makes aggregation occur drastically. Although PVP can coat on nanoparticles and forbid further aggregation, the exceeding high concentration of nanoparticles in a localized volume still results in severe aggregation. By adjusting the molar ratio of $PVP/AgNO_3$, the balance of nanoparticle yield and aggregation can be controlled. The role of PVP in our work includes electron donor and surfactant.
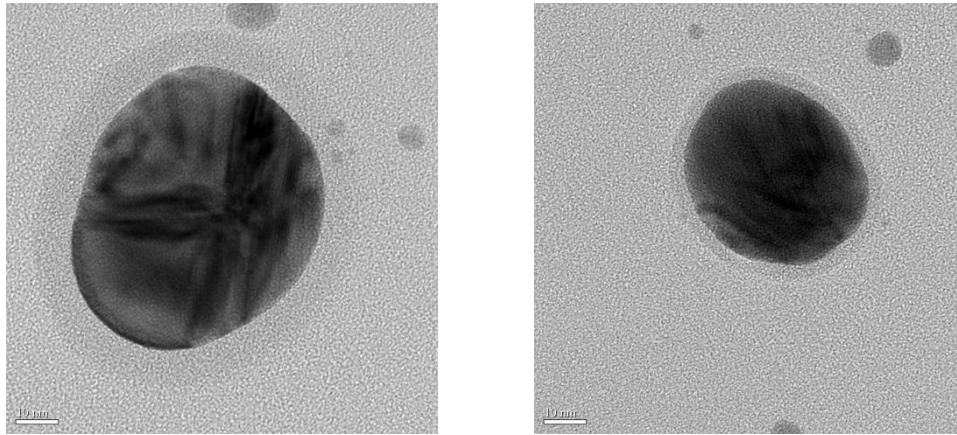
Fig.4.21 TEM image of silver nanoparticle covered with PVP around the surface as a layer. The molar ratio of PVP/AgNO$_3$ is 1 and irradiation time is 30 min.
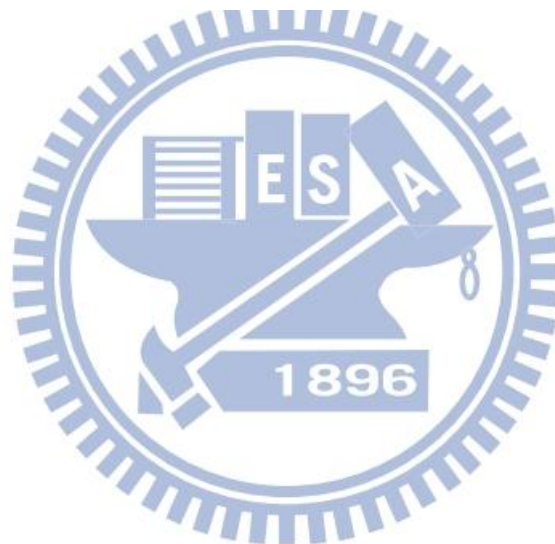
6. Conclusion

We have investigated the generation of transient chemical species for the reduction of $HAuCl_4$ and $AgNO_3$ in the presence/absence of PVP or 1-propanol. The formation of gold and silver nanoparticles was always monitored and confirmed by the change in extinction spectra of their surface plasmon.

The gold nanoparticle fabrication was investigated under three different experimental conditions with and without PVP, and 1-propanol. The laser energy dependence of gold nanoparticles suggested that the reduction of $HAuCl_4$ was achieved through 2-photon absorption of $AuCl_4^-$, which has unignorable absorption at 400 nm. SEM observation was carried out and the mean size of the obtained particles was estimated to be from 18 to 37 nm depending on experimental condition. Note that the colloidal solutions had high dispersability. Furthermore, we found that 1-propanol increases the reaction yield due to the stabilization for chloride radicals generated in the first step of chemical reaction of $AuCl_4^-$.

For silver nanoparticle fabrication, the Δextinction of the surface plasmon increased drastically only with PVP, while a little extinction change was observed without it. This result strongly supports that silver ions are reduced by PVP radicals through the 2-photon absorption. The meaningful result is that the slight change of the

Δextinction of the surface plasmon was observed even in the absence of any chemicals. This result implies that hydroxyl and/or hydrogen radicals due to 4-photon absorption of water reduces Ag ion to Ag atom.

From a different angle in this work, we have successfully demonstrated the metal nanoparticle fabrication by the combination of top-down and bottom-up methods of laser ablation and reduction, respectively. The mean size and size distribution were successfully controllable by tuning various kinds of laser parameter. Finally, we hope that our results will open a new door for not only study on femtosecond-laser chemistry but also novel fabrication method of metal nanoparticles.

7. References

1. Bauerle, D., *Laser Process and Chemistry*, Berlin :Springer, 2000.

2. Sugiyama, T.; Adachi, T.; Masuhara, H., Crystallization of Glycine by Photon Pressure of a Focused CW Laser Beam. *Chemistry Letters* 2007, *36* (12), 1480-1481.

3. Vogel, A.; Venugopalan, V., Mechanisms of Pulsed Laser Ablation of Biological Tissues. *Chemical Reviews* 2003, *103* (2), 577-644.

4. (a) Jain, P. K.; El-Sayed, I. H.; El-Sayed, M. A., Au nanoparticles target cancer. *Nano Today* 2007, *2* (1), 18-29; (b) Vogel, A.; Noack, J.; Hüttman, G.; Paltauf, G., Mechanisms of femtosecond laser nanosurgery of cells and tissues. *Applied Physics B: Lasers and Optics* 2005, *81* (8), 1015-1047.

5. Link, S.; El-Sayed, M. A., Shape and size dependence of radiative, non-radiative and photothermal properties of gold nanocrystals. *International Reviews in Physical Chemistry* 2000, *19* (3), 409-453.

6. (a) Sönnichsen, C. Plasmons in metal nanostructures. PhD Thesis, Ludwig-Maximilians-Universtät München, München, 2001; (b) Link, S.; El-Sayed, M. A., Spectral Properties and Relaxation Dynamics of Surface Plasmon Electronic Oscillations in Gold and Silver Nanodots and Nanorods. *The Journal of Physical Chemistry B* 1999, *103* (40), 8410-8426; (c) Sosa, I. O.; Noguez, C.; Barrera, R. G., Optical Properties of Metal Nanoparticles with Arbitrary Shapes. *The Journal of Physical Chemistry B* 2003, *107* (26), 6269-6275; (d) Jain, P. K.; Lee, K. S.; El-Sayed, I. H.; El-Sayed, M. A., Calculated Absorption and Scattering Properties of Gold Nanoparticles of Different Size, Shape, and Composition: Applications in Biological Imaging and Biomedicine. *The Journal of Physical Chemistry B* 2006, *110* (14), 7238-7248; (e) Sönnichsen, C.; Franzl, T.; Wilk, T.; von Plessen, G.; Feldmann, J.; Wilson, O.; Mulvaney, P., Drastic Reduction of Plasmon Damping in Gold Nanorods. *Physical Review Letters* 2002, *88* (7), 077402.

7. (a) Jung, B.; Jo, W.; Gwon, M. J.; Lee, E.; Kim, D. W., Scanning probe lithography for fabrication of Ti metal nanodot arrays. *Ultramicroscopy* 2010, *110* (6), 737-40; (b) Marrian, C. R. K.; Dobisz, E. A.; Dagata, J. A., ELECTRON-BEAM LITHOGRAPHY WITH THE SCANNING TUNNELING MICROSCOPE. *Journal of Vacuum Science & Technology B* 1992, *10* (6), 2877-2881.

8. Hohenau, A.; Ditlbacher, H.; Lamprecht, B.; Krenn, J. R.; Leitner, A.; Aussenegg, F. R., Electron beam lithography, a helpful tool for nanooptics. *Microelectronic Engineering* 2006, *83* (4-9), 1464-1467.

9. (a) Besner, S.; Kabashin, A. V.; Meunier, M., Fragmentation of colloidal nanoparticles by femtosecond laser-induced supercontinuum generation. *Applied*

Physics Letters 2006, *89* (23), 233122; (b) Werner, D.; Hashimoto, S.; Tomita, T.; Matsuo, S.; Makita, Y., Examination of Silver Nanoparticle Fabrication by Pulsed-Laser Ablation of Flakes in Primary Alcohols. *The Journal of Physical Chemistry C* 2008, *112* (5), 1321-1329; (c) Sylvestre, J.-P.; Poulin, S.; Kabashin, A. V.; Sacher, E.; Meunier, M.; Luong, J. H. T., Surface Chemistry of Gold Nanoparticles Produced by Laser Ablation in Aqueous Media. *The Journal of Physical Chemistry B* 2004, *108* (43), 16864-16869; (d) Tamaki, Y.; Asahi, T.; Masuhara, H., Nanoparticle Formation of Vanadyl Phthalocyanine by Laser Ablation of Its Crystalline Powder in a Poor Solvent†. *The Journal of Physical Chemistry A* 2002, *106* (10), 2135-2139; (e) Tsuji, T.; Thang, D. H.; Okazaki, Y.; Nakanishi, M.; Tsuboi, Y.; Tsuji, M., Preparation of silver nanoparticles by laser ablation in polyvinylpyrrolidone solutions. *Applied Surface Science* 2008, *254* (16), 5224-5230; (f) Sugiyama, T.; Asahi, T.; Takeuchi, H.; Masuhara, H., Size and Phase Control in Quinacridone Nanoparticle Formation by Laser Ablation in Water. *Japanese Journal of Applied Physics* 2006, *45* (1B), 384-388.

10. Nishi, T.; Suzuki, N.; Sugiyama, H.; Yano, K.; Azuma, H., High concentration silver nanoparticles stably dispersed in water without chemical reagent. *Journal of Photochemistry and Photobiology A: Chemistry* 2011, *226* (1), 64-67.

11. Kimling, J.; Maier, M.; Okenve, B.; Kotaidis, V.; Ballot, H.; Plech, A., Turkevich Method for Gold Nanoparticle Synthesis Revisited. *The Journal of Physical Chemistry B* 2006, *110* (32), 15700-15707.

12. Brust, M.; Walker, M.; Bethell, D.; Schiffrin, D. J.; Whyman, R., Synthesis of thiol-derivatised gold nanoparticles in a two-phase Liquid-Liquid system. *Journal of the Chemical Society, Chemical Communications* 1994, (7), 801-802.

13. Perrault, S. D.; Chan, W. C. W., Synthesis and Surface Modification of Highly Monodispersed, Spherical Gold Nanoparticles of 50−200 nm. *Journal of the American Chemical Society* 2009, *131* (47), 17042-17043.

14. (a) Okitsu, K.; Ashokkumar, M.; Grieser, F., Sonochemical Synthesis of Gold Nanoparticles: Effects of Ultrasound Frequency. *The Journal of Physical Chemistry B* 2005, *109* (44), 20673-20675; (b) Okitsu, K.; Yue, A.; Tanabe, S.; Matsumoto, H.; Yobiko, Y., Formation of Colloidal Gold Nanoparticles in an Ultrasonic Field: Control of Rate of Gold(III) Reduction and Size of Formed Gold Particles. *Langmuir* 2001, *17* (25), 7717-7720; (c) Caruso, R. A.; Ashokkumar, M.; Grieser, F., Sonochemical formation of colloidal platinum. *Colloids and Surfaces A: Physicochemical and Engineering Aspects* 2000, *169* (1–3), 219-225; (d) Mizukoshi, Y.; Oshima, R.; Maeda, Y.; Nagata, Y., Preparation of Platinum Nanoparticles by Sonochemical Reduction of the Pt(II) Ion. *Langmuir* 1999, *15* (8), 2733-2737; (e) Okitsu, K.; Bandow, H.; Maeda, Y.; Nagata, Y., Sonochemical Preparation of Ultrafine

Palladium Particles. *Chemistry of Materials* 1996, *8* (2), 315-317; (f) Sostaric, J. Z.; Mulvaney, P.; Grieser, F., Sonochemical dissolution of MnO2 colloids. *Journal of the Chemical Society, Faraday Transactions* 1995, *91* (17), 2843-2846; (g) Hobson, R. A.; Mulvaney, P.; Grieser, F., Formation of Q-state CdS colloids using ultrasound. *Journal of the Chemical Society, Chemical Communications* 1994, (7), 823-824; (h) Wang, G. Z.; Chen, W.; Liang, C. H.; Wang, Y. W.; Meng, G. W.; Zhang, L. D., Preparation and characterization of CdS nanoparticles by ultrasonic irradiation. *Inorganic Chemistry Communications* 2001, *4* (4), 208-210.

15. Rutherford, E., Cavitation hots up. *Nature* 2005, *434* (7029), 33-33.

16. Barber, B. P.; Hiller, R. A.; Löfstedt, R.; Putterman, S. J.; Weninger, K. R., Defining the unknowns of sonoluminescence. *Physics Reports* 1997, *281* (2), 65-143.

17. Flannigan, D. J.; Suslick, K. S., Plasma formation and temperature measurement during single-bubble cavitation. *Nature* 2005, *434* (7029), 52-55.

18. Didenko, Y. T.; Suslick, K. S., The energy efficiency of formation of photons, radicals and ions during single-bubble cavitation. *Nature* 2002, *418* (6896), 394.

19. Caruso, R. A.; Ashokkumar, M.; Grieser, F., Sonochemical Formation of Gold Sols. *Langmuir* 2002, *18* (21), 7831-7836.

20. Misra, N.; Biswal, J.; Gupta, A.; Sainis, J. K.; Sabharwal, S., Gamma radiation induced synthesis of gold nanoparticles in aqueous polyvinyl pyrrolidone solution and its application for hydrogen peroxide estimation. *Radiation Physics and Chemistry* 2012, *81* (2), 195-200.

21. Henglein, A.; Meisel, D., Radiolytic Control of the Size of Colloidal Gold Nanoparticles. *Langmuir* 1998, *14* (26), 7392-7396.

22. Pal, A., Photoinitiated gold sol generation in aqueous Triton X-100 and its analytical application for spectrophotometric determination of gold. *Talanta* 1998, *46* (4), 583-587.

23. Pal, A.; Esumi, K.; Pal, T., Preparation of nanosized gold particles in a biopolymer using UV photoactivation. *Journal of colloid and interface science* 2005, *288* (2), 396-401.

24. Mallik, K.; Mandal, M.; Pradhan, N.; Pal, T., Seed Mediated Formation of Bimetallic Nanoparticles by UV Irradiation: A Photochemical Approach for the Preparation of "Core−Shell" Type Structures. *Nano Letters* 2001, *1* (6), 319-322.

25. Kelly, K. L.; Coronado, E.; Zhao, L. L.; Schatz, G. C., The Optical Properties of Metal Nanoparticles: The Influence of Size, Shape, and Dielectric Environment. *The Journal of Physical Chemistry B* 2002, *107* (3), 668-677.

26. Fridman, A., *Plasma Chemistry*, New York: Cambidge, 2008.

27. Boulnois, J.-L., Photophysical processes in recent medical laser developments: A review. *LASERS IN MEDICAL SCIENCE* 1986, *1* (1), 47-66.

28. (a) Schaffer, C.; Nishimura, N.; Glezer, E.; Kim, A.; Mazur, E., Dynamics of femtosecond laser-induced breakdown in water from femtoseconds to microseconds. *Optics Express* 2002, *10* (3), 196-203; (b) Juhasz, T., Kastis, G.A., Suárez, C., Bor, Z. & Bron, W.E., Time-resolved observations of shock waves and cavitation bubbles generated by femtosecond laser pulses in corneal tissue and water. *Lasers in Surgery and Medicine* 1996, *19* (1), 23-31.

29. Huang, H. H.; Ni, X. P.; Loy, G. L.; Chew, C. H.; Tan, K. L.; Loh, F. C.; Deng, J. F.; Xu, G. Q., Photochemical Formation of Silver Nanoparticles in Poly(N-vinylpyrrolidone). *Langmuir* 1996, *12* (4), 909-912.

30. Nakamura, T.; Magara, H.; Herbani, Y.; Sato, S., Fabrication of silver nanoparticles by highly intense laser irradiation of aqueous solution. *Applied Physics A: Materials Science & Processing* 2011, *104* (4), 1021-1024.

31. (a) Kim, Y.-G.; Oh, S.-K.; Crooks, R. M., Preparation and Characterization of 1−2 nm Dendrimer-Encapsulated Gold Nanoparticles Having Very Narrow Size Distributions. *Chemistry of Materials* 2003, *16* (1), 167-172; (b) He, P.; Urban, M. W., Phospholipid-Stabilized Au−Nanoparticles. *Biomacromolecules* 2005, *6* (3), 1224-1225; (c) Esumi, K.; Suzuki, A.; Yamahira, A.; Torigoe, K., Role of Poly(amidoamine) Dendrimers for Preparing Nanoparticles of Gold, Platinum, and Silver. *Langmuir* 2000, *16* (6), 2604-2608.

32. Esumi, K.; Hara, J.; Aihara, N.; Usui, K.; Torigoe, K., Preparation of Anisotropic Gold Particles Using a Gemini Surfactant Template. *Journal of colloid and interface science* 1998, *208* (2), 578-581.

33. Pilar, F. L.; Higasi, K.; Baba, H.; Rembaum, A., *Quantum organic chemistry*, New York: Wiley, 1966.

34. Wang, T.; Zhu, Y.; Yang, K.; Ma, J. In *Two-Dimensional Silver Structures Fabricated by Two-Photon Femtolaser*, Optoelectronics and Image Processing (ICOIP), 2010 International Conference, 2010, 710-713.

35. Capek, I., *Nanocomposite structures and dispersions*, Amsterdam: Elsevier, 2006.

36. Zhao, T.; Sun, R.; Yu, S.; Zhang, Z.; Zhou, L.; Huang, H.; Du, R., Size-controlled preparation of silver nanoparticles by a modified polyol method. *Colloids and Surfaces A: Physicochemical and Engineering Aspects* 2010, *366* (1-3), 197-202.